the mTOR pathway regulate transforming growth factor-beta induced EMT [46] and that the inhibition of mTOR may be effective in intervention for EMT in chronic nephropathies [47]. In this study, treatment with everolimus abolished the accumulation of alpha-SMA in the tubulointerstitial space (Fig. 6). Furthermore, histological analysis revealed that the dilatation of proximal tubules was reduced by the treatment with everolimus (Fig. 5). These results suggest that the constitutively active mTOR pathway modulates dysfunction of proximal tubular epithelial cells via EMT in CRF.

In addition to improving renal tubular functions, everolimus also inhibited the accumulation of alpha-SMA (Fig. 6B and D) and infiltration of macrophages (Fig. 6F and H) without affecting the Ccr or the level of BUN (Table 1) when administration of everolimus was started at 8 weeks after Nx. These results are consistent with the report by Diekmann et al. [19] with another mTOR inhibitor, rapamycin. However, the effects of everolimus were rather complex when the administration was initiated at 2 weeks after renal ablation. Everolimus decreased Ccr and increased the level of BUN, but showed renoprotective effects as indicated by the decreased levels of alpha-SMA and ED1 (Fig. 6) and did not induce further albuminuria (Table 1). Because the hypertrophic responses are predominantly observed within 4 weeks after Nx [38], high doses of mTOR inhibitors could decrease single nephron-GFR and increased both afferent and efferent glomerular resistance without a reduction of whole kidney GFR in normal rat kidney [48]. Therefore, everolimus might cause further reductions of renal function in the rats during the vigorous compensative adaptation. However, further studies are needed to clarify the discrepancy in the pharmacological response to the inhibition of mTOR after Nx, and the limitation of mTOR inhibitors for CRF focusing on disease stage.

In summary, the constitutive activated mTOR pathway in the proximal tubules was revealed in the rat remnant kidneys. In addition, mTOR inhibitors had renoprotective effects to ameliorate progressive tubular dysfunction in the advanced stage of CRF. Although the precise molecular mechanisms of signal transduction in the progressive renal failure by which the inhibition of mTOR leads to these effects remain to be elucidated, these results suggested an additional therapeutic approach to end-stage renal disease with mTOR inhibitors focusing on the proximal tubular functions.

Acknowledgments

This work was supported in part by a grant-in-aid for Research on Biological Markers for New Drug Development, Health and Labour Sciences Research Grants from the Ministry of Health, Labour and Welfare of Japan (08062855 to S. Masuda), by the Japan Health Science Foundation "Research on Health Sciences Focusing on Drug Innovation" (KH23303 to S. Masuda), by a Grant-in-Aid for Scientific Research (A) (20249036 to K. Inui), Grant-in-Aid for Young Scientists (A) (18689016 to S. Masuda) and Grant-in-Aid for JSPS Fellows (20-2438 to K. Nishihara) from the Ministry of Education, Science, Culture, Sports and Technology of Japan (MEXT). K. Nishihara is a Research Fellow of the Japan Society for the Promotion of Science (JSPS).

References

[1] Taal MW, Brenner BM. Adaptation to nephron loss. In: Brenner BM, editor. The kidney. WB Saunders; 2008. p. 783–819.
[2] Remuzzi G, Bertani T. Pathophysiology of progressive nephropathies. N Engl J Med 1998;339:1448–56.
[3] Takeuchi A, Masuda S, Saito H, Doi T, Inui K. Role of kidney-specific organic anion transporters in the urinary excretion of methotrexate. Kidney Int 2001;60:1058–68.
[4] Ji L, Masuda S, Saito H, Inui K. Down-regulation of rat organic cation transporter rOCT2 by 5/6 nephrectomy. Kidney Int 2002;62:514–24.
[5] Horiba N, Masuda S, Takeuchi A, Saito H, Okuda M, Inui K. Gene expression variance based on random sequencing in rat remnant kidney. Kidney Int 2004;66:29–45.
[6] Nishihara K, Masuda S, Ji L, Katsura T, Inui K. Pharmacokinetic significance of luminal multidrug and toxin extrusion 1 in chronic renal failure rats. Biochem Pharmacol 2007;73:1482–90.
[7] Kwon TH, Frokiaer J, Fernandez-Llama P, Maunsbach AB, Knepper MA, Nielsen S. Altered expression of Na transporters NHE-3, NaPi-II, Na-K-ATPase, BSC-1, and TSC in CRF rat kidneys. Am J Physiol 1999;277:F257–70.
[8] Takahashi K, Masuda S, Nakamura N, Saito H, Futami T, Doi T, et al. Upregulation of H(+)-peptide cotransporter PEPT2 in rat remnant kidney. Am J Physiol Renal Physiol 2001;281:F1109–16.
[9] Sun H, Frassetto L, Benet LZ. Effects of renal failure on drug transport and metabolism. Pharmacol Ther 2006;109:1–11.
[10] Matsuzaki T, Watanabe H, Yoshitome K, Morisaki T, Hamada A, Nonoguchi H, et al. Downregulation of organic anion transporters in rat kidney under ischemia/reperfusion-induced acute renal failure. Kidney Int 2007;71:539–47.
[11] Fingar DC, Blenis J. Target of rapamycin (TOR): an integrator of nutrient and growth factor signals and coordinator of cell growth and cell cycle progression. Oncogene 2004;23:3151–71.
[12] Wullschleger S, Loewith R, Hall MN. TOR signaling in growth and metabolism. Cell 2006;124:471–84.
[13] Inoki K, Corradetti MN, Guan KL. Dysregulation of the TSC-mTOR pathway in human disease. Nat Genet 2005;37:19–24.
[14] Stallone G, Infante B, Schena A, Battaglia M, Ditonno P, Loverre A, et al. Rapamycin for treatment of chronic allograft nephropathy in renal transplant patients. J Am Soc Nephrol 2005;16:3755–62.
[15] Pontrelli P, Rossini M, Infante B, Stallone G, Schena A, Loverre A, et al. Rapamycin inhibits PAI-1 expression and reduces interstitial fibrosis and glomerulosclerosis in chronic allograft nephropathy. Transplantation 2008;85:125–34.
[16] Shillingford JM, Murcia NS, Larson CH, Low SH, Hedgepeth R, Brown N, et al. The mTOR pathway is regulated by polycystin-1, and its inhibition reverses renal cystogenesis in polycystic kidney disease. Proc Natl Acad Sci U S A 2006;103:5466–71.
[17] Nagai K, Matsubara T, Mima A, Sumi E, Kanamori H, Iehara N, et al. Gas6 induces Akt/mTOR-mediated mesangial hypertrophy in diabetic nephropathy. Kidney Int 2005;68:552–61.
[18] Lloberas N, Cruzado JM, Franquesa M, Herrero-Fresneda I, Torras J, Alperovich G, et al. Mammalian target of rapamycin pathway blockade slows progression of diabetic kidney disease in rats. J Am Soc Nephrol 2006;17:1395–404.
[19] Diekmann F, Rovira J, Carreras J, Arellano EM, Banon-Maneus E, Ramirez-Bajo MJ, et al. Mammalian target of rapamycin inhibition halts the progression of proteinuria in a rat model of reduced renal mass. J Am Soc Nephrol 2007;18:2653–60.
[20] Vogelbacher R, Wittmann S, Braun A, Daniel C, Hugo C. The mTOR inhibitor everolimus induces proteinuria and renal deterioration in the remnant kidney model in the rat. Transplantation 2007;84:1492–9.
[21] Yokomasu A, Yano I, Sato E, Masuda S, Katsura T, Inui K. Effect of intestinal and hepatic first-pass extraction on the pharmacokinetics of everolimus in rats. Drug Metab Pharmacokinet 2008;23:469–75.
[22] Masuda S, Saito H, Nonoguchi H, Tomita K, Inui K. mRNA distribution and membrane localization of the OAT-K1 organic anion transporter in rat renal tubules. FEBS Lett 1997;407:127–31.
[23] Ichimura T, Bonventre JV, Bailly V, Wei H, Hession CA, Cate RL, et al. Kidney injury molecule-1 (KIM-1), a putative epithelial cell adhesion molecule containing a novel immunoglobulin domain, is up-regulated in renal cells after injury. J Biol Chem 1998;273:4135–42.
[24] Ogihara H, Saito H, Shin BC, Terado T, Takenoshita S, Nagamachi Y, et al. Immuno-localization of H+/peptide cotransporter in rat digestive tract. Biochem Biophys Res Commun 1996;220:848–52.
[25] Takahashi K, Nakamura N, Terada T, Okano T, Futami T, Saito H, et al. Interaction of beta-lactam antibiotics with H+/peptide cotransporters in rat renal brush-border membranes. J Pharmacol Exp Ther 1998;286:1037–42.
[26] Urakami Y, Okuda M, Masuda S, Saito H, Inui K. Functional characteristics and membrane localization of rat multispecific organic cation transporters, OCT1 and OCT2, mediating tubular secretion of cationic drugs. J Pharmacol Exp Ther 1998;287:800–5.
[27] Urakami Y, Nakamura N, Takahashi K, Okuda M, Saito H, Hashimoto Y, et al. Gender differences in expression of organic cation transporter OCT2 in rat kidney. FEBS Lett 1999;461:339–42.
[28] Hashida T, Masuda S, Uemoto S, Saito H, Tanaka K, Inui K. Pharmacokinetic and prognostic significance of intestinal MDR1 expression in recipients of living-donor liver transplantation. Clin Pharmacol Ther 2001;69:308–16.
[29] Tao Y, Kim J, Schrier RW, Edelstein CL. Rapamycin markedly slows disease progression in a rat model of polycystic kidney disease. J Am Soc Nephrol 2005;16:46–51.
[30] Chen JK, Chen J, Neilson EG, Harris RC. Role of mammalian target of rapamycin signaling in compensatory renal hypertrophy. J Am Soc Nephrol 2005;16:1384–91.
[31] Andreucci M, Fuiano G, Presta P, Esposito P, Faga T, Bisesti V, et al. Radiocontrast media cause dephosphorylation of Akt and downstream signaling targets in human renal proximal tubular cells. Biochem Pharmacol 2006;72:1334–42.

[32] Mariappan MM, Shetty M, Sataranatarajan K, Choudhury GG, Kasinath BS. Glycogen synthase kinase 3beta is a novel regulator of high glucose- and high insulin-induced extracellular matrix protein synthesis in renal proximal tubular epithelial cells. J Biol Chem 2008;283:30566–75.
[33] Birn H, Christensen EI. Renal albumin absorption in physiology and pathology. Kidney Int 2006;69:440–9.
[34] Russo LM, Sandoval RM, Campos SB, Molitoris BA, Comper WD, Brown D. Impaired tubular uptake explains albuminuria in early diabetic nephropathy. J Am Soc Nephrol 2009;20:489–94.
[35] Letavernier E, Bruneval P, Vandermeersch S, Perez J, Mandet C, Belair MF, et al. Sirolimus interacts with pathways essential for podocyte integrity. Nephrol Dial Transplant 2009;24:630–8.
[36] Boron WF. Acid-base transport by the renal proximal tubule. J Am Soc Nephrol 2006;17:2368–82.
[37] Inui K, Masuda S, Saito H, Cellular. molecular aspects of drug transport in the kidney. Kidney Int 2000;58:944–58.
[38] Motohashi H, Sakurai Y, Saito H, Masuda S, Urakami Y, Goto M, et al. Gene expression levels and immunolocalization of organic ion transporters in the human kidney. J Am Soc Nephrol 2002;13:866–74.
[39] Urakami Y, Akazawa M, Saito H, Okuda M. Inui K. cDNA cloning, functional characterization, and tissue distribution of an alternatively spliced variant of organic cation transporter hOCT2 predominantly expressed in the human kidney. J Am Soc Nephrol 2002;13:1703–10.
[40] Masuda S, Terada T, Yonezawa A, Tanihara Y, Kishimoto K, Katsura T, et al. Identification and functional characterization of a new human kidney-specific H+/organic cation antiporter, kidney-specific multidrug and toxin extrusion 2. J Am Soc Nephrol 2006;17:2127–35.
[41] van Timmeren MM, Bakker SJ, Vaidya VS, Bailly V, Schuurs TA, Damman J, et al. Tubular kidney injury molecule-1 in protein-overload nephropathy. Am J Physiol Renal Physiol 2006;291:F456–64.
[42] Ichimura T, Asseldonk EJ, Humphreys BD, Gunaratnam L, Duffield JS, Bonventre JV. Kidney injury molecule-1 is a phosphatidylserine receptor that confers a phagocytic phenotype on epithelial cells. J Clin Invest 2008;118:1657–68.
[43] Kalluri R, Neilson EG. Epithelial-mesenchymal transition and its implications for fibrosis. J Clin Invest 2003;112:1776–84.
[44] Kliem V, Johnson RJ, Alpers CE, Yoshimura A, Couser WG, Koch KM, et al. Mechanisms involved in the pathogenesis of tubulointerstitial fibrosis in 5/6-nephrectomized rats. Kidney Int 1996;49:666–78.
[45] Ng YY, Huang TP, Yang WC, Chen ZP, Yang AH, Mu W, et al. Tubular epithelial-myofibroblast transdifferentiation in progressive tubulointerstitial fibrosis in 5/6 nephrectomized rats. Kidney Int 1998;54:864–76.
[46] Lamouille S, Derynck R. Cell size and invasion in TGF-beta-induced epithelial to mesenchymal transition is regulated by activation of the mTOR pathway. J Cell Biol 2007;178:437–51.
[47] Wu MJ, Wen MC, Chiu YT, Chiou YY, Shu KH, Tang MJ. Rapamycin attenuates unilateral ureteral obstruction-induced renal fibrosis. Kidney Int 2006;69:2029–36.
[48] Sabbatini M, Sansone G, Uccello F, De Nicola L, Nappi F, Andreucci VE. Acute effects of rapamycin on glomerular dynamics: a micropuncture study in the rat. Transplantation 2000;69:1946–90.

Heterozygous variants of multidrug and toxin extrusions (MATE1 and MATE2-K) have little influence on the disposition of metformin in diabetic patients

Kana Toyama[a], Atsushi Yonezawa[a], Masahiro Tsuda[a], Satohiro Masuda[a], Ikuko Yano[a], Tomohiro Terada[a], Riyo Osawa[a], Toshiya Katsura[a], Masaya Hosokawa[b], Shimpei Fujimoto[b], Nobuya Inagaki[b] and Ken-Ichi Inui[a]

Multidrug and toxin extrusions (MATE1/SLC47A1 and MATE2-K/SLC47A2) play important roles in the renal excretion of metformin. We have previously identified the nonsynonymous *MATE* variants with functional defects at low allelic frequencies. The purpose of this study was to evaluate the effects of heterozygous *MATE* variants on the disposition of metformin in mice and humans. Pharmacokinetic parameters of metformin in *Mate1*(±) heterozygous mice were comparable with those in *Mate1*(+/+) wild-type mice. Among 48 Japanese diabetic patients, seven patients carried heterozygous *MATE* variant and no patient carried homozygous *MATE* variant. There was no significant difference in oral clearance of metformin with or without heterozygous *MATE* variants. In addition, creatinine clearance, but not heterozygous *MATE* variants, significantly improved the model fit of metformin clearance by statistical analysis using the nonlinear mixed-effects modeling program. In conclusion, heterozygous *MATE* variants could not influence the disposition of metformin in diabetic patients. *Pharmacogenetics and Genomics* 20:135–138 © 2010 Wolters Kluwer Health | Lippincott Williams & Wilkins.

Pharmacogenetics and Genomics 2010, **20**:135–138

Keywords: creatinine clearance, H^+/organic cation antiporter, metformin, organic cation transporter, pharmacokinetics

[a]Department of Pharmacy, Faculty of Medicine, Kyoto University Hospital and [b]Department of Diabetes and Clinical Nutrition, Graduate School of Medicine, Kyoto University, Sakyo-ku, Kyoto, Japan

Correspondence to Professor Ken-ichi Inui, PhD, Department of Pharmacy, Kyoto University Hospital, Sakyo-ku, Kyoto 606-8507, Japan
Tel: +81 75 751 3577; fax: +81 75 751 4207;
e-mail: inui@kuhp.kyoto-u.ac.jp

Received 17 September 2009 **Accepted** 16 November 2009

Metformin is widely used for the treatment of hyperglycemia in patients with noninsulin-dependent diabetes mellitus. The major pharmacological action of metformin involves the suppression of gluconeogenesis in the liver. Lactic acidosis is a rare but serious adverse effect of metformin, which occurs predominantly in patients with renal insufficiency. Clinical pharmacokinetic studies revealed that metformin is mainly excreted into urine in an unchanged form without hepatic metabolism, and that the renal clearance of metformin is approximately five times higher than creatinine clearance (Ccr) [1], suggesting that renal tubular secretion is a major route of metformin elimination. In human proximal tubules, multidrug and toxin extrusion 1 (MATE1/SLC47A1) and a kidney-specific isoform MATE2-K/SLC47A2 are localized at the brush-border membranes, which were characterized as H^+/organic cation antiporters [2]. In rodents, Mate1, but not Mate2, is expressed in the kidney [2]. Metformin is a substrate for MATE1 and MATE2-K, as well as organic cation transporter 2 (OCT2/SLC22A2), which is localized at the basolateral membranes of the kidney [2,3]. The functional significance of MATE in the kidney was previously shown using *Mate1* knockout mice [4]. On the basis of these backgrounds and findings, MATE1 and MATE2-K could play key roles in metformin tubular secretion in humans.

Genetic variants in *MATE* genes are likely to be one of the factors for interindividual variability in metformin pharmacokinetics and pharmacodynamics. Recently, we and another group identified nonsynonymous single nucleotide polymorphisms (SNPs) in coding region of *MATE* genes, some of which reduced the transport activity [5,6]. In addition, Becker *et al.* [7] reported that rs2289669G > A SNP in the *MATE1* gene was associated with the glucose-lowering effect, but metformin pharmacokinetics was not evaluated. Tzvetkov *et al.* [8] demonstrated that there was no relationship between the same SNP and metformin pharmacokinetics. However, rs2289669G > A SNP in the *MATE1* gene was located in noncoding intron region and there was no information about the effect of this non-coding SNP on the transport activity. Therefore, it is not clear whether the functional reduced nonsynonymous *MATE* variants alter metformin disposition. The allelic frequencies of all *MATE* variants were quite low, in the range of 0.6–2.4% [5,6]. Homozygous variants with functional loss of transport activity decrease drug elimination in most

Supplemental digital content is available for this article. Direct URL citations appear in the printed text and are provided in the HTML and PDF versions of this article on the journal's Website (*www.pharmacogeneticsandgenomics.com*).

1744-6872 © 2010 Wolters Kluwer Health | Lippincott Williams & Wilkins

DOI: 10.1097/FPC.0b013e328335639f

cases. The effect of heterozygous variants, in contrast, depends on the transporters and the drugs. In the breast cancer resistance protein (*BCRP/ABCG2*) gene, heterozygous Q141K variant caused elevated oral bioavailability of its substrate [9]. These results suggested that information about the influence of heterozygous as well as homozygous *MATE* variants on metformin pharmacokinetics is required for its safe use in clinical situations. In this study, therefore, we focused on the effect of heterozygous nonsynonymous *MATE* variants on metformin disposition in diabetic patients.

Using *Mate1*(+/+) wild-type, *Mate1*(±) heterozygous and *Mate1*(−/−) homozygous mice, we first examined the pharmacokinetics of metformin (Supplemental methods, Supplemental digital content 1 *http://links.lww.com/FPC/A82*). High plasma concentration and low urinary excretion of metformin were observed in *Mate1*(−/−) mice compared with *Mate1*(+/+) mice, whereas there was no difference between *Mate1*(±) and *Mate1*(+/+) mice (Fig. 1a and b). In addition, several pharmacokinetic parameters in *Mate1*(±) mice were comparable with those in *Mate1*(+/+) mice (Supplemental Table 1, Supplemental digital content 2 *http://links.lww.com/FPC/A83*). Mate1 protein expression levels in these three genotype mice are shown in Fig. 1c. The transport of metformin by HEK293 cells expressing mouse Mate1, mouse Oct1 or mouse Oct2 was confirmed (Supplemental Fig. 1, Supplemental digital content 3 *http://links.lww.com/FPC/A84*). Based on these results, we hypothesized that the heterozygous *MATE* variants do not influence on the metformin clearance in humans as well as in mice.

To address the species difference in *MATE* genes, pharmacokinetic evaluation was also carried out in humans. Forty-eight Japanese patients with diabetes mellitus were enrolled into this study. Blood samples were obtained at 0, 4, and 9 h after metformin administration, followed by the determination of plasma concentrations and genotype for *MATE1*, *MATE2-K*, and *OCT2* genes (Supplemental methods, Supplemental digital content 1 *http://links.lww.com/FPC/A82*). The oral clearance (CL/F) of metformin in diabetic patients was estimated by the empirical Bayesian method with the nonlinear mixed-effects modeling program NONMEM using a basic model: CL/F=θ1. Two MATE1-G64D variant carriers, two MATE1-L125F variant carriers, and one MATE1-D328A variant carrier were found in this study. In the *MATE2-K* gene, the G211V variant was found in two patients. All *MATE* variant carriers were heterozygotes and included in the *MATE*-heterozygous variant group. The plasma concentration–time profile after an oral administration of metformin in *MATE*-heterozygous variant group was similar to that in *MATE*-reference group (Supplemental Fig. 2, Supplemental digital content 4 *http://links.lww.com/FPC/A85*). Patient

Fig. 1

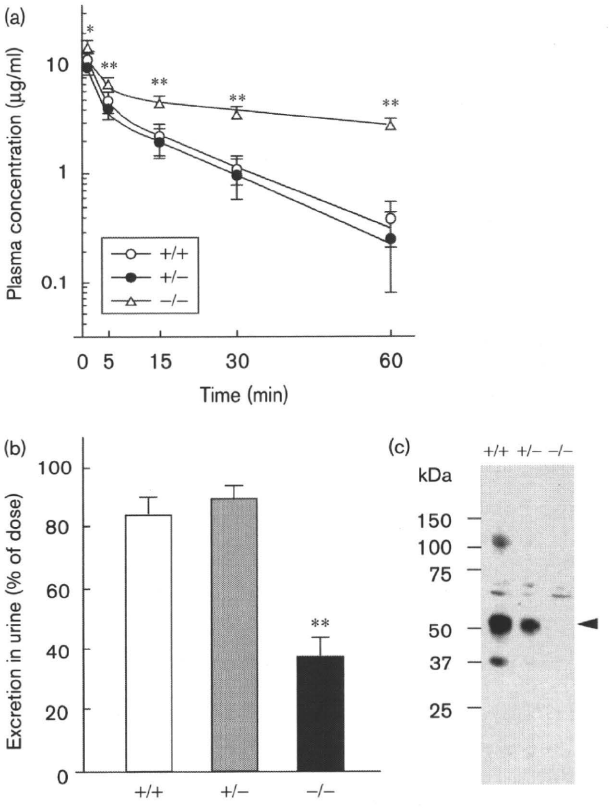

Metformin pharmacokinetic studies of *Mate1*(+/+), *Mate1*(±), and *Mate1*(−/−) mice. (a) Plasma concentration–time profiles were obtained after the intravenous administration of metformin to *Mate1* (+/+) (open circles), *Mate1*(±) (closed circles), and *Mate1*(−/−) (open triangles) mice. (b) Urinary excretion of metformin in *Mate1* (+/+) (open column), *Mate1*(±) (gray column), and *Mate1*(−/−) (closed column) mice were calculated using urine samples collected for 60 min after the drug administration. Each column represents the mean ± SD for six to eight mice. $*P<0.05$, $**P<0.01$, significantly different from *Mate1*(+/+) mice. (c) Western blot analysis of Mate1 in renal brush-border membrane fractions was carried out. The arrowhead indicates the position of mouse Mate1.

characteristics were similar between the two groups. There was no statistically significant difference in metformin CL/F between the *MATE*-heterozygous variant group and the *MATE*-reference group (Table 1). All of 11 *OCT2* variant carriers were also heterozygotes. Only one patient carried both MATE1-G64D and OCT2-A270S variants. The CL/F values of the *MATE*-variant group, the *OCT2*-variant group and both the *MATE*-variant and *OCT2*-variant group were comparable with those of the reference group (Supplemental Table 2, Supplemental digital content 5 *http://links.lww.com/FPC/A86*).

To determine the most important factor contributing to interindividual variability in metformin CL/F, we examined the relationship between CL/F and patient characteristics, such as age, sex, renal function, and

Table 1 Patient characteristics and effects of heterozygous *MATE* variants on metformin oral clearance in 48 Japanese patients with diabetes mellitus

	MATE reference	MATE-heterozygous variant[a]
Patients	41	7
Sex (male/female)	17/24	1/6
Age (years)	62±10	67±8
BMI (kg/m^2)	27±4	25±3
Metformin CL/F (ml/min)	603±137	658±115
Ccr (ml/min)	98±34	83±37
eGFR (ml/min)	71±23	71±21

Ccr, 24-h creatinine clearance; CL/F, oral clearance of metformin; eGFR, estimated glomerular filtration rate; MATE, multidrug and toxin extrusion.
[a]*MATE*-heterozygous variant includes MATE1-G64D ($n=2$), MATE1-L125F ($n=2$), MATE1-D328A ($n=1$), MATE2-K-G211V ($n=2$). No patient carried other *MATE* variants; MATE1-V10L, MATE1-A310V, MATE1-V338I, MATE1-N474S, MATE1-V480M, MATE1-C497S, MATE1-Q519H, and MATE2-K-K64N. Data are expressed as mean±SD. There was no statistically significant difference between two groups.

transporter genetic variations. Regression analysis showed that metformin CL/F was positively correlated with both Ccr and estimated glomerular filtration rate (eGFR) (Supplemental Fig. 3, Supplemental digital content 6 *http://links.lww.com/FPC/A87*). In NONMEM analysis, model fit was significantly improved for the models using the individual Ccr or eGFR compared with the basic model (CL/F=θ1). However, there was no improvement in the models with age, sex or genetic variants of the *MATE* or *OCT2* gene. A negative of twice the log likelihood difference (−2LLD) value was higher in the model using Ccr than that using eGFR (Supplemental Table 3, Supplemental digital content 7 *http://links.lww.com/FPC/A88*). The incorporation of Ccr into the basic model explained part of the interindividual variability in CL/F, with its value decreasing from 26.1 to 19.6%.

Interindividual variability in MATE activity is likely to affect the pharmacokinetics of metformin. Examination with *Mate1* knockout mice strongly suggested the pharmacokinetic alternation in humans with the functional defect homozygous variants [4]. However, homozygous variants in *MATE1* and *MATE2-K* genes were reported to be quite rare [5,6]. Therefore, we examined the pharmacokinetic significance of the heterozygous *MATE* variants to clarify whether we should pay attention to these genotypes in the clinical situations. As expected from the animal data, the heterozygous *MATE* variants did not affect the disposition of metformin in humans (Fig. 1 and Table 1). The rate-limiting step in the renal secretion of metformin is either the renal blood flow, the tubular uptake across the basolateral membranes or efflux into the lumen at the brush-border membranes. In this study, heterozygous *MATE* variants did not affect metformin clearance, although MATE1 and MATE2-K were important for metformin secretion [2,3]. Likewise, heterozygous *OCT2* variant did not affect metformin clearance in diabetic patients, even though the pharmacokinetic effect of *OCT2* variant is still controversial [3,8,10]. The renal clearance of metformin was reported to be in the range of 335–615 ml/min in humans [1], which is comparable with renal plasma flow. These results suggested that renal blood flow is a rate-limiting factor for metformin secretion. Therefore, heterozygous *MATE* variants possibly show only a minor portion in the interindividual variation of metformin pharmacokinetics in clinical situations.

For determination of the most important factor contributing to metformin disposition among age, sex, renal function, and heterozygous variations of *MATE* and *OCT2* genes, NONMEM analysis was carried out. Consistent with previous reports [1,8], we showed that Ccr is a significant predictor of metformin clearance. Although Ccr is used clinically as a marker of GFR, Ccr is known to overestimate GFR because of the creatinine tubular secretion. Previously, we showed that creatinine is a substrate for OCT2, MATE1, and MATE2-K [2]. These reports suggested that creatinine as well as metformin is excreted into the urine by tubular secretion through organic cation transport systems in addition to glomerular filtration. Comparable with these findings, metformin CL/F had a higher correlation with Ccr than with eGFR. Therefore, Ccr is the most clinical reliable indicator of metformin disposition.

In conclusion, it was shown that heterozygous *MATE* variants as well as heterozygous *OCT2* variants do not affect metformin disposition in diabetic patients. Moreover, it was revealed that Ccr is the most important factor to predict metformin disposition in the clinical use. On account of the low allelic frequency, further studies are needed with much more patients to determine the effect of homozygous *MATE* variants on metformin disposition in clinical situations.

Acknowledgements

The authors are grateful to all the medical staff of Department of Diabetes and Clinical Nutrition, Graduate School of Medicine, Kyoto University, especially to Dr Chizumi Yamada, Dr Kazuyo Fujita, Dr Akio Obara, Dr Norio Harada, Dr Kazutaka Nagai, and Dr Shiho Takahara for excellent help. This study was supported in part by a grant-in-aid for Scientific Research (KAKENHI) from the Ministry of Education, Science, Culture, and Sports of Japan. M. Tsuda is a Research Fellow of the Japan Society for the Promotion of Science.

References

1 Scheen AJ. Clinical pharmacokinetics of metformin. *Clin Pharmacokinet* 1996; **30**:359–371.
2 Terada T, Inui K. Physiological and pharmacokinetic roles of H^+/organic cation antiporters (MATE/SLC47A). *Biochem Pharmacol* 2008; **75**:1689–1696.
3 Takane H, Shikata E, Otsubo K, Higuchi S, Ieiri I. Polymorphism in human organic cation transporters and metformin action. *Pharmacogenomics* 2008; **9**:415–422.

4 Tsuda M, Terada T, Mizuno T, Katsura T, Shimakura J, Inui K. Targeted disruption of the multidrug and toxin extrusion 1 (Mate1) gene in mice reduces renal secretion of metformin. *Mol Pharmacol* 2009; **75**:1280–1286.
5 Kajiwara M, Terada T, Ogasawara K, Iwano J, Katsura T, Fukatsu A, *et al.* Identification of multidrug and toxin extrusion (MATE1 and MATE2-K) variants with complete loss of transport activity. *J Hum Genet* 2009; **54**:40–46.
6 Chen Y, Teranishi K, Li S, Yee SW, Hesselson S, Stryke D, *et al.* Genetic variants in multidrug and toxic compound extrusion-1, hMATE1, alter transport function. *Pharmacogenomics J* 2009; **9**:127–136.
7 Becker MSL, Visser LE, van Schaik RHN, Hofman A, Uitterlinden AG, Stricker BHC. Genetic variation in the multidrug and toxin extrusion 1 transporter protein influences the glucose-lowering effect of metformin in patients with diabetes: a preliminary study. *Diabetes* 2009; **58**:745–749.
8 Tzvetkov MV, Vormfelde SV, Balen D, Meineke I, Schmidt T, Sehrt D, *et al.* The effects of genetic polymorphisms in the organic cation transporters OCT1, OCT2, and OCT3 on the renal clearance of metformin. *Clin Pharmacol Ther* 2009; **86**:299–306.
9 Sparreboom A, Gelderblom H, Marsh S, Ahluwalia R, Obach R, Principe P, *et al.* Diflomotecan pharmacokinetics in relation to ABCG2 421C>A genotype. *Clin Pharmacol Ther* 2004; **76**:38–44.
10 Chen Y, Li S, Brown C, Cheatham S, Castro RA, Leabman MK, *et al.* Effect of genetic variation in the organic cation transporter 2 on the renal elimination of metformin. *Pharmacogenet Genomics* 2009; **19**:497–504.

J. Biochem. 2010;148(5):557–563 doi:10.1093/jb/mvq087

JB THE JOURNAL OF BIOCHEMISTRY

Time-saving multiplex detection of single nucleotide polymorphisms by ultrasensitive DNA microarray

Received April 21, 2010; accepted July 27, 2010; published online August 16, 2010

Makiko Ichikawa[1,*], Keishi Miwa[1], Tomo Yamasaki[1], Izumi Nakagawa[1], Satoko Takizawa[1], Satohiro Masuda[2] and Ken-ichi Inui[2]

[1]Toray Industries, Inc., New Frontiers Research Laboratories, 6-10-1, Tebiro, Kamakura, Kanagawa 248-0036 and [2]Department of Pharmacy, Kyoto University Hospital, Sakyo-ku, Kyoto 606-8507, Kyoto, Japan

*Makiko Ichikawa, Toray Industries, Inc., New Frontiers Research Laboratories, 6-10-1, Tebiro, Kamakura, Kanagawa, 248-0036, Japan. Tel: +81 467 32 8947, Fax: +81 467 32 8364, email: makiko_ichikawa@nts.toray.co.jp

Rapid and multiplex detection system using an ultrasensitive DNA microarray was developed and utilized for the analysis of six pharmacokinetically relevant single nucleotide polymorphisms (SNPs) (*MDR1*-C1236T, *MDR1*-G2677TA, *MDR1*-C3435T, *CYP3A5*-A6986G, *CYP2C19*-G681A, *CYP2C19*-G636A) from blood samples derived from liver transplant patients. The SNP detection system is comprised of three processes: multiplex PCR, single base extension with fluorescently labelled di-deoxy-nucleotides and detection by DNA microarray. The entire workflow of this system completes within 5 h. The final genotype call was obtained statistically by Mahalanobis distance which was calculated from the bi-coloured fluorescent signals detected by the microarray. In order to detect the six SNPs, this system required only 50 copies of genomic DNA, and the obtained detection calls completely matched with the results by the sequencing-based genotyping method. With the high sensitivity and rapid processing, our SNP detection system utilizing ultrasensitive microarray is a promising device applicable for diagnostic utility.

Keywords: diagnostic tool/microarray/multiplex/SNP/transplantation.

Abbreviations: CYP, cytochrome P450; ddNTP, di-deoxy NTP; MDR, multidrug resistance; PMT, Photo Multiplier Tube; POCT, point of care testing; PPI, proton pomp inhibitor; SBE, single base extention; SNP, single nucleotide polymorphism.

Our knowledge of the human genome has increased rapidly in recent decades due to the completion of the Human Genome Project and other large-scale endeavours, and these discoveries are now applied for personalized medicine and genome-based drug discovery.

Calcineurin inhibitor tacrolimus (FK-506) has been used as a primary immuno- suppressive agent in liver transplantation (*1*). Proton pump inhibitors (PPIs) are often co-administrated with tacrolimus in patients receiving allograft transplantation to avoid surgical stress-related gastric bleeding or gastrointestinal ulceration. However, this co-administration sometimes adversely affects the concentration/dose (C/D) ratio of tacrolimus, which leads to side effects such as nephrotoxicity, neurotoxicity and life-threatening infection (*2*, *3*). It is known that the pharmacokinetics of tacrolimus attributes to individual genomic variation (*4–6*). As previously reported, PPIs are primarily metabolized by the cytochrome P450 subfamilies CYP2C19 and CYP3A4 (*7*, *8*). Tacrolimus is metabolized by CYP3A4 and CYP3A5 and pumped out of the cell membrane by multi-drug resistance 1 protein (MDR1/ABCB1) (Fig. 1) (*9–11*). Because CYP3A4 on the metabolic pathway is shared by both PPIs and tacrolimus, the competitive metabolism is influenced by the molecule activities on the collateral metabolic pathway, *CYP3A5*, *CYP2C19* and *MDR1* (Fig. 1). In clinical practice, the rapid and multiplex genotyping system is required in case such as the administration of tacrolimus.

Several technologies have been developed for the SNP detection system. The most accurate and commonly used SNP detection system is a direct sequencing of target gene regions; however, a sequencing technology needs long operation time over one working day and is not suitable for multiplex genotyping. Other systems are also commercially available such as SNPstream® by Beckman Coulter (*12*) and GeneChip® by Affimetrix (*13*), which are suitable for highly multiplexed analysis. On the other hand, we have previously developed an ultrasensitive DNA microarray based on three unique technologies: a black plastic substrate, a columnar array structure and a micro-bead agitation system. Due to these properties, the signal/noise ratio was markedly improved, achieving 100-fold higher sensitivity than that of conventional glass-supported microarrays (*14*).

In the present study, we focused on developing a new SNP detection assay in a compact system, more suitable for a clinical setting for personalized pharmacotherapy by the compact system. We developed multiplex and rapid genotyping system using an ultrasensitive DNA microarray with the SBE method for the analysis of six pharmacokinetically relevant SNPs (*MDR1*-C1236T, *MDR1*-G2677TA,

MDR1-C3435T, *CYP3A5*-A6986G, *CYP2C19*-G681A and *CYP2C19*-G636A). The entire workflow of this system completes within 5 h and specific with only 50 copies of genome. Using this system, we analyzed genomic DNA isolated from the blood of 83 liver transplant patients. The genotyping results were validated with the sequencing-based genotyping method.

Materials and Methods

Patients and DNA extraction

A total of 83 Japanese living-donor liver transplant patients, including donors and recipients were enrolled in this study (*6*). Prior to use, all DNA samples were anonymized using unlinked numbers. Written informed consent was obtained from all study participants prior to enrolment. This study was conducted in accordance with the Declaration of Helsinki and its amendments, and was approved by the Kyoto University Graduate School of Medicine Ethics Committee, as well as Human Genome Ethics Committee for R&D, Toray Industries, Inc.

Human genomic DNA was extracted from whole blood using a Wizard Genomic DNA Purification Kit (Promega Co., Madison, WI, USA), and the extracted DNA was dissolved in distilled water and stored at −30°C. The genomic DNA of cultured cells was extracted from HEK 293 cells using the QIAamp DNA Mini Kit (QIAGEN, Germantown, MD, USA), and the extracted DNA was dissolved in distilled water and stored at −30°C.

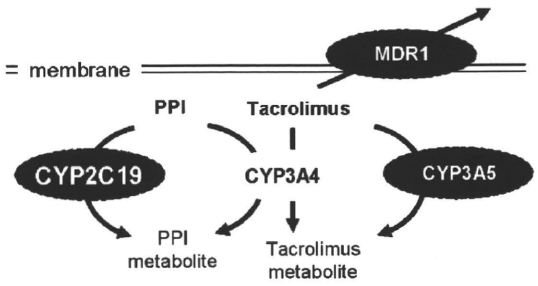

Fig. 1 Transport and metabolic pathway of Tacrolimus and PPI.

Oligonucleotides

Multiplex PCR primers were synthesized for the amplification of six regions including six SNPs. SBE primers designed to have each unique tag sequence were synthesized (Table I). Additionally, two pairs of control template (Control 1, 2) and SBE primers (Control 1SBE, 2SBE) were designed for the standardization of Cyanine (Cy) 3 and Cy5 fluorescence intensity, and another two pairs of control template (Control 3G, 4C) and SBE primers (Control 3SBE, 4SBE) were designed to monitor for dNTP contamination in SBE reaction (Table II). To hybridize SBE primers onto the DNA microarray, eleven unique tag-probes of 20 mer nucleotides, which were complementary to the SBE primer's tag sequence, were also synthesized. The 3' end of each tag-probe was aminated. All nucleotides were synthesized by Operon Biotechnologies (Tokyo, Japan).

Multiplex PCR and SBE reaction

Six regions of genomic DNA were simultaneously amplified by multiplex PCR, which include three SNPs of *MDR1* (C1236T, G2677TA and C3435T), one SNP of *CYP3A5* (A6986G) and two SNPs of *CYP2C19* (G681A and G636A). The amplification was performed in a reaction solution that consisted of 0.2 mM each deoxy-nucleotide (dNTP), 1.5 mM magnesium sulphate, 0.3 μM forward and reverse primers, 1.0 U KOD plus DNA polymerase (Toyobo Co. Ltd, Tokyo, Japan) and 10 pg to 100 ng of genomic DNA, adjusted to 50 μL with KOD-Plus-Vers.2 buffer. These mixtures were applied to a thermal cycler PCR system (ABI9700, Applied Biosystems, Foster City, CA, USA) and denatured at 94°C for 2 min followed by 30 PCR cycles (94°C for 30 s, 58°C for 30 s and 68°C for 1 min). Following the PCR reaction, free dNTPs were removed from the PCR products using GFX PCR DNA and a Gel Band Purification Kit (GE Healthcare UK Ltd, UK). The size of the amplicons was measured with a 2100 bioanalyzer system (Agilent Technologies, Inc., USA).

The SBE reaction was performed in 20 μL of reaction mixture containing 15 nM of each SBE primer, except in the case of control reactions, which contained Control 1SBE primer (7.5 nM) and control 3SBE primer (3.75 nM): 5 μL of reaction buffer, 2 μL of purified multiplex PCR product; 2.5 ng of each control template (except Control 1A (7.5 ng) and Control 1G (5.0 ng)); 500 nM each of Cy 5 labelled di-deoxy-UTP (ddUTP), Cy3-ddCTP, Cy5-ddGTP and Cy3-ddATP (PerkinElmer Inc., Boston, MA, USA); 500 nM of di-deoxy-nucleotides (ddNTPs); and 5 units of ThermoSequenase DNA Polymerase (GE Healthcare Life Science, USA). The assay was conducted in two separate tubes. The first tube, which was used for the detection of A or G SNP, contained purified multiplex PCR amplicons, SBE primers (MDR1-1236, MDR1-2677-1, MDR1-3435, CYP2C19-636, Control 1SBE primer and Control

Table I. Sequences of optimized primers for multiplex PCR amplification and for single-base extension assay at each SNP position.

SNP position	Primers	Sequences
MDR1-1236C/T	Forward	5′-AACAGTCAGTTCCTATATCCTGTGTC-3′
	Reverse	5′-CAGCTGGACTGTTGTGCTCTTCCC-3′
	SBE	5′-ACTCGTCCTGGTAGATCTTGAAGGG-3′
MDR1-2677G/T/A	Forward	5′-CCCATCATTGCAATAGCAGGAGT-3′
	Reverse	5′-GAGCATAGTAAGCAGTAGGGAG-3′
	SBE 1	5′-ATCATATTTAGTTTGACTCACCTTCCCAG-3′
	SBE 2	5′-ATCATATTTAGTTTGACTCACCTTCCCAG-3′
MDR1-3435C/T	Forward	5′-ACTGCAGCATTGCTGAGAACATTGCCT-3′
	Reverse	5′-CATTAGGCAGTGACTCGATGAAGGCAT-3′
	SBE	5′-AGCCGGGTGGTGTCACAGGAAGAGAT-3′
CYP3A5-6986A/G	Forward	5′-TGGCATAGGAGATACCCAC-3′
	Reverse	5′-TTCATATGATGAAGGGTAATGTG-3′
	SBE	5′-CTCTTTAAAGAGCTCTTTTGTCTTTCA-3′
CYP2C19-681G/A	Forward	5′-TGCAATAATTTTCCCACTATCATT-3′
	Reverse	5′-TACGCAAGCAGTCACATAACTAAG-3′
	SBE	5′-ATAATTTTCCCACTATCATTGATTATTTCCC-3′
CYP2C19-636G/A	Forward	5′-GAAAAATTGAATGAAAACATCAGG-3′
	Reverse	5′-TGCCATCTTTTCCAGATATTCACC-3′
	SBE	5′-GGAAGCAAAAAACTTGGCCTTACCTGGAT-3′

Forward: Forward primer for PCR amplification, Reverse: Reverse Primer for PCR amplification. SBE: Primer for single-base extension. The 5′ end of each primer was attached to an original tag sequence (not shown).

Table II. Sequence of control templates and control primers for single base extension assay.

Name	Sequences
Control 1	5′-TCTGCAGGTCAGGGGGGCAAGAAGGGGTAACCCAGGTGTCACTGAAGATTGTA"X"AGATTTGGGGAATGTTGCAGTATTTGAAAGTGCTCCACCAAAGCT-3′ X: A or G
Control 2	5′-GTAAGTGGAGCCTGATTTCCCTAAGGACTTCTGGTTTGCTCTT"X"AAGAAAGCTGTGCCCCAGAACACCAGAGACCTCAAATTACTTTACAAATAGAA-3′ X: T or C
Control 3G	5′-TACCATTTTAAAGGCTATCATTACTCTTTACCTGTGAAGAG"G"AGAACATGAAGAAATCTACTTTATTCAGATATTCTCCAGATTCCTAAAGATTAGAGAT-3′
Control 4C	5′-GTATAGCTCTGTGAAACCATTTGCAAATTTTTTGAATAGG"C"TAAGTTATAGCAGATACAACAGGTTGGGCACTGGATATATAAAGATAAACAAAATATAG-3′
Control 1 SBE	5′-TCAAATACTGCAACATTCCCCAAATCT-3′
Control 2 SBE	5′-TGGTGTTCTGGGGCACAGCTTTCTT-3′
Control 3 SBE	5′-TATTAATAAAGTAGATTTCTTCATGTTCT-3′
Control 4 SBE	5′-AACCTGTTGTATCTGCTATAACTTA-3′

Control: control SNPs template. "X" is the detection position of each SBE primer. SBE: Primer for single-base extention. The 5′ end of each primer is attached to an original tag sequence (not shown).

3SBE primer), control templates (1A, 1G and 3G), Cy3-ddCTP, Cy5-ddUTP, ddGTP, ddATP, reaction buffer and thermo sequenase polymerase. The second tube, which was used for the detection of T or C SNP, contained purified multiplex PCR amplicons, SBE primers (MDR1-2677-2, CYP3A5-6986, CYP2C19-681, Control 2SBE primer and Control 4SBE primer), control templates (2C, 2T and 4C), Cy3-ddATP, Cy5-ddGTP, ddCTP, ddUTP, reaction buffer and thermo sequenase polymerase. Heat denaturation at 95°C for 2 min was followed by 30 cycles of PCR reaction (95°C for 20 s and 60°C for 15 s).

The specificity of the SBE reaction was confirmed by the single signal intensity of Control 3SBE primer (Cy3) or Control 4SBE primer (Cy5). Control 1SBE primer with Cy5-ddUTP, Control 1SBE primer with Cy3-ddCTP, Control 2SBE primer with Cy5-ddGTP, and Control 2SBE primer with Cy3-ddATP were used to standardize the signal intensities of each nucleotide. These controls calibrated the enzyme reaction efficiency and the scanner's PMT gain.

Determination of SNPs with the microarray

The DNA microarray platform for 256 spots was provided by Toray Industries, Inc. Eleven unique oligonucleotide sequences that were not complementary to the human genome were selected as tag probes to capture the SNPs specific tagged detection primer. These tagged probes were covalently immobilized to the surface of the microarray as previously reported (*6*). 5 μL of each SBE reaction tubes was mixed with 30 μL of 3D-Gene™ hybridization buffer (Toray Industries, Inc., Tokyo, Japan) and was applied onto the DNA microarray. Then, the DNA microarray was placed in a hybridization chamber (TaKaRa Hybridization Chamber 5 No.TX711, TaKaRa Bio, Japan), and rotated horizontally at 42°C for 1.5 h at 250 rpm. After hybridization, the microarrays were washed and dried. The hybridized microarrays were scanned on a microarray scanner (ScanArray Express, PerkinElmer, Inc., USA) to measure fluorescence intensity. At a laser power setting of 60%, the photomultiplier sensitivity was adjusted so that the fluorescence signal intensities from the two fluorophores, Cy3 and Cy5, at the gain control spots on the microarray were almost comparable.

The ratio of Cy3 and Cy5 signal intensity (Cy3/Cy5, R) was log translated and used as a calibration factor (Log_2(R)) to standardize the signal intensities of each SNP. We used two reaction tubes and two sets of control template and SBE primers. For reaction tube 1, R was calculated as $R_1 = (Scy3/SCon1cy3)/(Scy5/SCon1cy5)$ where Scy3 and SCon1cy3 are the Cy3 signal intensity of the sample and of Control 1, and Scy5 and SCon1cy5 are the Cy5 signal intensity of the sample and of Control 1, respectively. The Cy3 signal intensity of Control 1SBE primer with Cy3-ddCTP was used for the calibration of the Cy3 signal intensity of MDR1-1236, MDR1-2677-1, MDR1-3435 and CYP2C19-636, and the Cy5 of Control 1SBE primer with Cy5-ddUTP was used for the calibration of the Cy5 signal intensity of MDR1-1236, MDR1-2677, MDR1-3435 and CYP2C19-636, respectively.

For reaction tube 2, R was calculated as $R_2 = (Scy3/SCon2cy3)/(Scy5/SCon2cy5)$ where Scy3 and SCon2cy3 are the Cy3 signal intensity of the sample and of Control 2, and Scy5 and SCon2cy5 are the Cy5 signal intensity of the sample and of Control 2, respectively. The Cy3 signal intensity of the Control 2_SBE primer with Cy3-ddATP was used for the calibration of the Cy3 signal intensity of MDR1-2677-2, CYP3A5-6986, and CYP2C19-681, and the Cy5 signal of Control 2SBE primer with Cy5-ddGTP was used for the calibration of the Cy5 signal intensity of MDR1-2677-2, CYP3A5-6986, and CYP2C19-681, respectively. The whole procedure, consisting of genome extraction, multiplexed PCR, SBE and detection by DNA microarray, is illustrated in Fig. 2.

Classification

As reported previously (*15*), genotype calls were made according to their Mahalanobis distance (D). All of $\log_2(R)$ values obtained from the training group (63 patients) were plotted and were separated into clusters (Fig. 3). The clusters were statistically validated by Dunnett test as well-defined clusters. The group centre (m) and the dispersion parameter (s) of each cluster were calculated. D was calculated using the $\log_2(R)$ value of test sample (x), as follows: $D^2 = (x - m)^2/s^2$. The genotypes of the samples were assigned to the cluster that provided the minimum D.

Direct sequencing using DNA sequencer

The nucleotide sequences of the PCR products were also measured by direct DNA sequencing using the BigDye Terminator v3.1 cycle sequencing kit (Applied Biosystems, Foster City, CA, USA). The PCR conditions outlined above were used for the amplification of SNP-containing DNA fragments in an ABI 2720 thermal cycler (Applied Biosystems), before being sequenced using an ABI PRISM 3100 Genetic Analyzer (Applied Biosystems).

Results

Multiplex PCR condition was examined using the genomic DNA of HEK293 cells, which provide six DNA fragments including pharmacokinetically relevant SNPs (*MDR1*-C1236T, *MDR1*-G2677TA, *MDR1*-C3435T, *CYP3A5*-A6986G, *CYP2C19*-G681A and *CYP2C19*-G636A). The multiplex PCR conditions and primer sequences were optimized to obtain a similar amplification yield of each amplicon and to distinguish molecular length of each amplicon, which ranged from 120 to 218 bp in length (Table I) by electrophoretic separation.

For the multiplex SBE reaction, several combinations of detection primer as well as labelled ddNTPs were tested to obtain the optimal conditions for

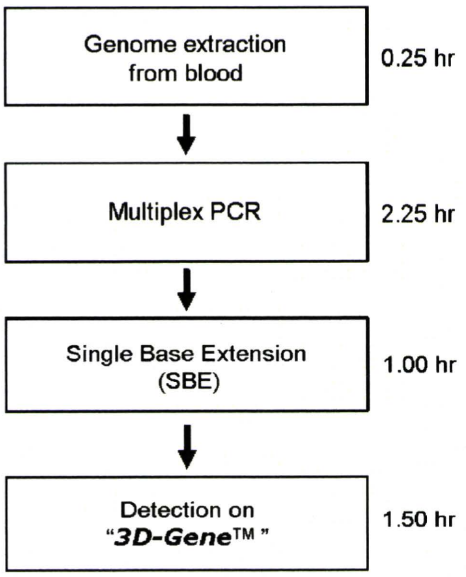

Fig. 2 Workflow and time course of the multiplex SNP detection by SBE reaction and 3D-Gene™ DNA microarray substrate.

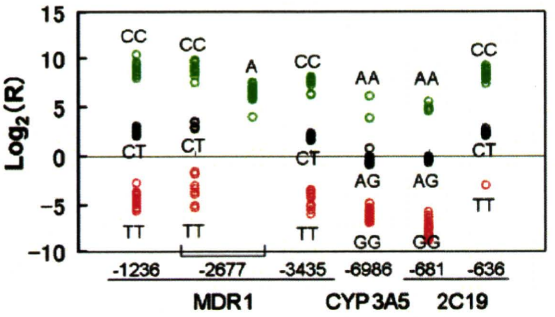

Fig. 3 Clusters based on log_2(R) values. Each SNP in a multiplex assay results in three clusters. The plot shows 476 data points from 68 patient genomes. The green circles represent CC(*MDR1*-1236, -2677 and -3435, *CYP2C19*-636) or AA(*MDR1*-2677, *CYP3A5*-6986 and *CYP2C19*-681) homozygous genotype, and the red circles represent TT(*MDR1*-1236, -2677 and -3435, *CYP2C19*-636) or GG(*CYP3A5*-6986 and *CYP2C19*-681) homozygous genotype. The black circles represent the heterozygous genotype CT(*MDR1*-1236, -2677 and -3435, *CYP2C19*-636) or GA(*CYP3A5*-6986 and *CYP2C19*-681).

distinguishing the six different SNPs. As a result, seven primers were selected and are presented as Table I.

The total handling time from collection of blood samples to analysis all six SNPs was minimized to 5 h, which includes 0.25 h for extraction, 2.25 h for multiplex PCR and 1 h for SBE reaction, followed by 1.5 h hybridization (Fig. 2).

For the standardization of fluorescence intensities, two pairs of control templates (Control 1 and 2) and two SBE primers (control 1SBE and 2SBE) were used (Table II). Each pair of control templates was identical in sequence except one nucleotide which is the artificial SNP. Following the SBE reaction and DNA microarray hybridization, the Cy3 and Cy5 fluorescence intensities of each artificial SNP standardized that of each sample SNP, as described under 'Determination of SNPs with microarray' in the 'Materials and Methods' section.

To validate whether SBE reactions were contaminated with free dNTPs, the control template (Control 3G or 4C) and a SBE primer (control 3SBE or 4SBE) were used. For example, if Cy5 fluorescence was detected when Control 3G, control 3SBE primer, Cy3-ddCTP and Cy5-ddUTP were assayed in a single tube, the SBE reaction was determined to be erroneous.

The genomic DNA of 63 Japanese living-donor liver transplant pairs, including donors and recipients, were used to investigate genomic polymorphisms in *CYP3A5*, *CYP2C19* and *MDR1*. All of the 63 genomic DNA samples were amplified by multiplex PCR and were detected for all six SNPs by our detection system.

These 63 samples were used as training data to construct a cluster map. As shown in Fig. 3, the log transformed signal intensity ratio ($log_2(R)$) of each sample was clearly separated into three clusters. These clusters corresponded to the genotypes (Fig. 3). In the case of *MDR1*-2677, four clusters were separated, because three types of SNPs——C, T and A might be available. The SBE primer MDR1-2677-1 discriminates CC or CT or TT, and MDR1-2677-2 discriminates AA or no signal. If MDR1-2677-1 detects TT and MDR1-2677-2 detects AA, the genotype would be TA.

Twenty additional genomic DNA samples were measured as a test group to confirm the accuracy of our SNP detection system. The 20 samples were measured by the SNP detection microarray and each Log_2(R) value and its Mahalanobis distance were calculated. These genotyping results were also measured by a capillary electrophoresis sequencer (ABI PRISM 3100), using the same PCR amplicons for 120 SNPs (six SNPs in 20 samples). Due to indistinct peaks in chromatogram by the direct sequencing (Fig. 4B), SNPs were detected in only 97 runs (81%) (Fig. 5). Failure of genotyping by direct sequencing may have been attributable to difficulties in multiplex PCR, as the amplicon yields were lower in the failed samples than those of successfully determined samples. These 23 problematic SNPs were identified by re-sequencing with PCR products amplified separately for each SNP. Conversely, the SNP detection microarray provided clear clusters and 119 data points (99%) were perfectly in accordance with sequencing results (Fig. 5). The one failed call for *MDR1*-3435 (sample ID:44) was identified following a fresh genomic DNA extraction.

To ascertain the sensitivity of our SNP detection system, 2 genomic DNA samples were randomly selected from samples of known genotype. The 2 samples of 1 μg each were subjected to 10-fold serial dilution and their genetic polymorphisms were measured at 100, 10, 1 ng and 100 pg amounts of genomic DNA. All six SNPs were detected from the samples containing only 100 pg of genomic DNA, which corresponds to approximately 50 genomic copies (Table III). Direct sequencing failed to genotype samples containing 100 pg of genomic DNA because of weak fluorescence signal intensity.

Discussion

In the clinical setting, the detection system for SNPs should be quick, precise and multiplex. We developed a multiplex genotype detection system based upon the ultrasensitive DNA microarray technology, and evaluated its performance using six SNPs relating to drug metabolism.

We first optimized the reaction conditions of multiple SNP analysis for both amplification and SBE, using genomic DNA derived from HEK293 cells. As a result, we identified an optimal combination of PCR primer sequences and SBE primer sequences as well as labelled ddNTPs. When a SNP could not be detected with the sense strand sequence, the anti-sense strand sequence was used for the SBE reaction, and this process was effective at distinguishing all six SNPs analysed. After optimizing these conditions, six SNPs were measured in 63 clinical samples by DNA microarrays. The genotyping result was validated with the sequencing-based genotyping method. We regarded these 63 clinical samples results as a training set. For the genotypic discrimination, we used the training set and adopted Mahalanobis distance for statistical calling of the genotypes. The genotype of new sample was assigned to the group by the shortest Mahalanobis distance. We evaluated our detection system using six SNPs of new 20 samples. The concordance rate of genotyping 120 SNPs by our detection system was 99%. Although one sample failed the detection of a SNP in *MDR1*-3435, re-purification of genomic DNA resulted in the correct detection of the SNPs in this sample, suggesting DNA degradation as a cause of incorrect genotyping. Over the course of this study, some genomic DNA samples were stored for longer than one year. In a clinical diagnostic setting, most of the blood sample would be treated within a few days of sampling and the sample quality should be ensured by the appropriate handling. Therefore, degradation of genomic DNA would not likely occur in the clinical setting.

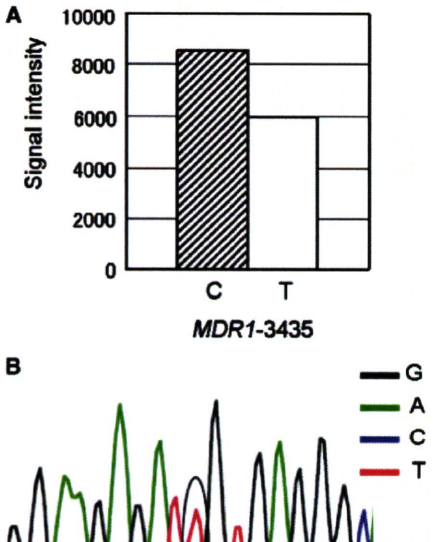

Fig. 4 A typical mismatched result of genotyping results obtained by DNA microarray and direct sequencing (sample ID:31, *MDR1*-3435). (A) Signal intensity of DNA microarray. The signal for Cy3 (striped bar-Cystein) shows 'C'. and Cy5 (open bar-Thymine) shows 'T', which show that this site is CT. (B) Electropherogram of the direct sequencing. The automated sequencing call was homozygotes TT.

In this study, we focused on developing a new SNP detection assay in a compact system, more suitable for a clinical setting for personalized pharmacotherapy by the compact system. As a primary step to develop an automated bed-side SNP-detection system constructed with the DNA microarray and the preprocessing lab-on-a-chip, we tried to find the minimum amount of DNA required for SNP detection by our system. In this study, the six SNPs were detected using only 100 pg of genomic DNA, which corresponds to 50 copies of genomic DNA obtained from 0.1 μL of blood. The required quantity of genomic DNA for this analysis is even less than SNPstream® (1~2 ng) and Infinium® HD BeadChip (200~400 ng).

Employing the highly sensitive DNA microarray substrate also enabled significant timesaving in SNP

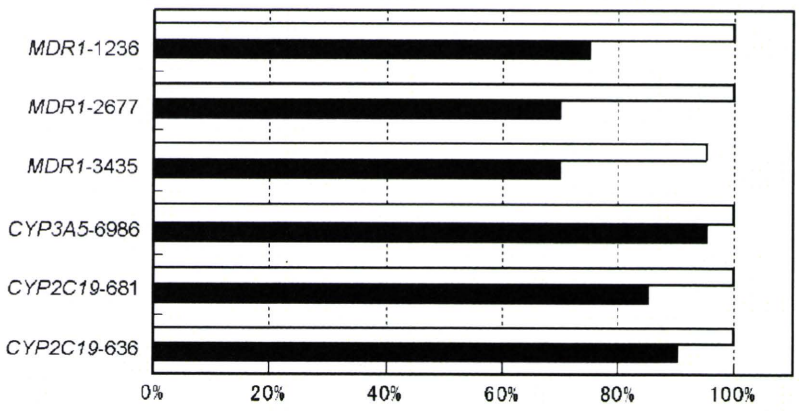

Fig. 5 Genotyping results by DNA microarray (open bar) or sequencing (closed bar) of the same amplicons amplified from 20 patients genome. The DNA microarray correctly distinguishes 100% of genotypes except for one SNP in *MDR1*-3435. The concordance rates by Sequencing are 70~95%, depending on the SNPs.

Table III. Representative results of the clusterization.

SNP position	$Log_2(R)$	Calculated by Mahalanobis distance			Judge
MDR1-1236	2.7	CC:79.0	CT:0.4	TT:132.4	CT
MDR1-2677-1	3.5	CC:69.1	CT:0.5	TT:41.4	CT
MDR1-3435	2.6	CC:64.1	CT:13.6	TT:62.4	CT
CYP3A5-6986	−0.7	AA:12.3	AG:0.0	GG:34.9	AG
CYP2C19-681	−10.8	AA:2637.6	AG:5073.0	GG:15.4	GG
CYP2C19-636	2.6	CC:314.0	CT:1.9	NC	CT

Genotyping judgements of six SNPs calculated by Mahalanobis distance. The $log_2(R)$ was calculated as shown in the 'Materials and methods' section. For the 'judge' calls, each SNP was assigned to the cluster with the smallest Mahalanobis distance. NC: No samples classified to the group.

detection. The hybridization reaction with the microarray is completed within 1.5 h, resulting in a total detection time of 5 h (Fig. 2). The short handling time is particularly suitable to use at the bedside. The substrate of this DNA microarray has been introduced by Nagino *et al.* (*14*) for the detection of the gene expression profiling. Nagino *et al.* showed that it takes 16 h for the hybridization of labelled cDNA to microarray probes. On the other hand, in our study it takes only 1.5 h for the hybridization. We suggest that one of the reasons for shortening of the hybridization is the difference of the length of labelled target nucleotides. The length of labelled cDNA used in Nagino's trial might range from several hundreds to several thousands mer; however, the tag-probe used in this study include polynucleotides of only 20 mer.

The genotypes of the *CYP3A5*, *CYP2C19* and *MDR1* genes were found to affect the pharmacokinetics of tacrolimus after liver transplantation (*4–6*, *9–11*). As the genotypes between the graft liver (donor) and native intestine (recipients) may be very different, it is necessary to detect the SNPs in DNA samples from both donor and recipients. As in the case of co-administration of tacrolimus and other drugs, risk evaluation by the point of care testing (POCT) is needed to prevent unexpected side-effects. Our SNP detection system which is sensitive and timesaving is suitable to the POCT.

On the other hand, SNPs related to various drug metabolism events are not limited to those shown in this study. The advantage of the SBE system on DNA microarray is its flexibility. By designing the sequence of PCR primers and SBE tagged primers, the number of detectable SNPs can be easily expanded. The system evaluated in this study could be increased to 256 tags for a sample.

In conclusion, the newly developed ultrasensitive DNA microarray achieved high sensitivity and accuracy for multiplex SNP genotyping. For further study, we are developing a lab-on-a-chip that enables automatic DNA isolation, labelling and hybridization to shorten the measurement time to within 3 h, avoid human-error and make it available at the clinical bedside.

Funding

This work was supported in part by New Energy and Industrial Technology Development Organization (NEDO) through 'Development of Practical Biological Tools'.

Conflict of interest

M.I., K.M., T.Y., I.N. and S.T. are employees of Toray Industries, Inc. Other authors have declared no conflict of interest.

References

1. Scott, L.J., McKeage, K., Keam, S.J., and Plosker, G.L. (2003) Tacrolimus: a further update of its use in the management of organ transplantation. *Drugs* **63**, 1247–1297
2. Yasuhara, M., Hashida, T., Toraguchi, M., Hashimoto, Y., Kimura, M., Inui, K., Inomata, I., Tanaka, K., and Yamaoka, Y. (1995) Pharmacokinetics and pharmacodynamics of FK 506 in pediatric patients receiving living-related donor liver transplantations. *Transplant Proc.* **27**, 1108–1110
3. Jusko, W.J., Piekoszewski, W., Klintmalm, G.B., Shaefer, M.S., Hebert, M.F., Piergies, A.A., Lee, C.C., Schechter, P., and Mekki, Q.A. (1995) Pharmacokinetics of tacrolimus in liver transplant patients. *Clin. Pharmacol. Ther.* **57**, 281–290
4. Itagaki, F., Homma, M., Yuzawa, K., Nishimura, M., Naito, S., Ueda, N., Ohkohchi, N., and Kohda, Y. (2004) Effect of lansoprazole and rabeprazole on tacrolimus pharmacokinetics in healthy volunteers with CYP2C19 mutations. *J. Pharm. Pharmacol.* **56**, 1055–1059
5. Takahashi, K., Motohashi, H., Yonezawa, A., Okuda, M., Ito, N., Yamamoto, S., Ogawa, O., and Inui, K. (2004) Lansoprazole-tacrolimus interaction in Japanese transplant recipient with CYP2C19 polymorphism. *Ann. Pharmacother.* **38**, 791–794
6. Hosohata, K., Masuda, S., Ogura, Y., Oike, F., Takada, Y., Katsura, T., Uemoto, S., and Inui, K. (2008) Interaction between tacrolimus and lansoprazole, but not rabeprazole in living-donor liver transplant patients with defects of CYP2C19 and CYP3A5. *Drug Metab. Pharmacokinet* **23**, 134–138
7. Yasuda, S., Horai, Y., Tomono, Y., Nakai, H., Yamato, C., Manabe, K., Kobayashi, K., Chiba, K., and Ishizaki, T. (1995) Comparison of the kinetic disposition and metabolism of E3810, a new proton pump inhibitor, and omeprazole in relation to S-mephenytoin 4′-hydroxylation status. *Clin. Pharmacol. Ther.* **58**, 143–154
8. Pearce, R.E., Rodrigues, A.D., Goldstein, J.A., and Parkinson, A. (1996) Identification of the human P450 enzymes involved in lansoprazole metabolism. *J. Pharmacol. Exp. Ther.* **277**, 805–816
9. Uesugi, M., Masuda, S., Katsura, T., Oike, F., Takada, Y., and Inui, K. (2006) Effect of intestinal CYP3A5 on postoperative tacrolimus trough levels in living-donor liver transplant recipients. *Pharmacogenet. Genomics* **16**, 119–127
10. Masuda, S., Goto, M., Fukatsu, S., Uesugi, M., Ogura, Y., Oike, F., Kiuchi, T., Takada, Y., Tanaka, K., and

Inui, K. (2006) Intestinal MDR1/ABCB1 level at surgery as a risk factor of acute cellular rejection in living-donor liver transplant patients. *Clin. Pharmacol. Ther.* **79**, 90–102
11. Wang, J., Zeevi, A., McCurry, K., Schuetz, E., Zheng, H., Iacono, A., McDade, K., Zaldonis, D., Webber, S., Watanabe, R.M., and Burckart, G.J. (2006) Impact of ABCB1 (MDR1) haplotypes on tacrolimus dosing in adult lung transplant patients who are CYP3A5 *3/*3 non-expressors. *Transpl. Immunol.* **15**, 235–240
12. Bell, P.A., Chaturvedi, S., Gelfand, C.A., Huang, C.Y., Kochersperger, M., Kopla, R., Modica, F., Pohl, M., Varde, S., Zhao, R., Zhao, X., and Boyce-Jacino, M.T. (2002) SNPstream UHT: ultra-high throughput SNP genotyping for pharmacogenomics and drug discovery. *Biotechniques* **32**, S70–S77
13. Hardenbol, P., Banér, J., Jain, M., Nilsson, M., Namsaraev, E.A., Karlin-Neumann, G.A., Fakhrai-Rad, H., Ronaghi, M., Willis, T.D., Landegren, U., and Davis, R.W. (2003) Multiplexed genotyping with sequence-tagged molecular inversion probes. *Nat. Biotechnol.* **21**, 673–678
14. Nagino, K., Nomura, O., Takii, Y., Myomoto, A., Ichikawa, M., Nakamura, F., Higasa, M., Akiyama, H., Nobumasa, H., Shiojima, S., and Tsujimoto, G. (2006) Ultrasensitive DNA chip: gene expression profile analysis without RNA amplification. *J. Biochem.* **139**, 697–703
15. Rabbee, N. and Speed, T.P. (2006) A genotype calling algorithm for affymetrix SNP arrays. *Bioinformatics* **22**, 7–12

Research article

Loss of the BMP antagonist USAG-1 ameliorates disease in a mouse model of the progressive hereditary kidney disease Alport syndrome

Mari Tanaka,[1] Misako Asada,[2] Atsuko Y. Higashi,[1] Jin Nakamura,[2] Akiko Oguchi,[2] Mayumi Tomita,[3] Sachiko Yamada,[1] Nariaki Asada,[2] Masayuki Takase,[2] Tomohiko Okuda,[4] Hiroshi Kawachi,[5] Aris N. Economides,[6] Elizabeth Robertson,[7] Satoru Takahashi,[8] Takeshi Sakurai,[9] Roel Goldschmeding,[10] Eri Muso,[11] Atsushi Fukatsu,[3] Toru Kita,[1] and Motoko Yanagita[1,2,3]

[1]Department of Cardiovascular Medicine, [2]Career-Path Promotion Unit for Young Life Scientists, [3]Department of Artificial Kidneys, and [4]COE Formation, Graduate School of Medicine, Kyoto University, Kyoto, Japan. [5]Department of Cell Biology, Institute of Nephrology, Niigata University Graduate School of Medical and Dental Sciences, Niigata, Japan. [6]Regeneron Pharmaceuticals Inc., Tarrytown, New York. [7]Wellcome Trust Center for Human Genetics, University of Oxford, Oxford, United Kingdom. [8]Laboratory Animal Resource Center, Institute of Basic Medical Sciences, University of Tsukuba, Ibaraki, Japan. [9]Department of Molecular Neuroscience and Integrative Physiology, Graduate School of Medical Science, Kanazawa University, Kanazawa, Japan. [10]Department of Pathology, University Medical Center Utrecht, Utrecht, Netherlands. [11]Division of Nephrology and Dialysis, Department of Medicine, Kitano Hospital, Osaka, Japan.

The glomerular basement membrane (GBM) is a key component of the filtering unit in the kidney. Mutations involving any of the collagen IV genes (*COL4A3*, *COL4A4*, and *COL4A5*) affect GBM assembly and cause Alport syndrome, a progressive hereditary kidney disease with no definitive therapy. Previously, we have demonstrated that the bone morphogenetic protein (BMP) antagonist uterine sensitization–associated gene-1 (USAG-1) negatively regulates the renoprotective action of BMP-7 in a mouse model of tubular injury during acute renal failure. Here, we investigated the role of USAG-1 in renal function in *Col4a3*$^{-/-}$ mice, which model Alport syndrome. Ablation of Usag1 in *Col4a3*$^{-/-}$ mice led to substantial attenuation of disease progression, normalization of GBM ultrastructure, preservation of renal function, and extension of life span. Immunohistochemical analysis revealed that USAG-1 and BMP-7 colocalized in the macula densa in the distal tubules, lying in direct contact with glomerular mesangial cells. Furthermore, in cultured mesangial cells, BMP-7 attenuated and USAG-1 enhanced the expression of MMP-12, a protease that may contribute to GBM degradation. These data suggest that the pathogenetic role of USAG-1 in *Col4a3*$^{-/-}$ mice might involve crosstalk between kidney tubules and the glomerulus and that inhibition of USAG-1 may be a promising therapeutic approach for the treatment of Alport syndrome.

Introduction

The renal glomerular basement membrane (GBM) contributes importantly to maintenance of the structural integrity of the glomerular capillaries (1, 2). Type IV collagen is the major component of the GBM, and its mutations have been linked to the genetic disorder Alport syndrome, a progressive hereditary kidney disease associated with sensorineural deafness (3). With a genetic frequency of about 1 in 5,000 people, it counts among the more prevalent of known genetic disorders (4). The disease is caused by the mutations in any one of the genes encoding the α3, α4, and α5 chains of type IV collagen (*COL4A3*, *COL4A4*, and *COL4A5*) (5–7), and a mutation affecting 1 of these chains forming the α3/α4/α5(IV) collagen network can alter or abolish the GBM expression not only of the corresponding chain but also of the other 2 chains (8). The GBM in Alport syndrome instead retains the fetal α1/α1/α2(IV) collagen network (9), which confers an increased susceptibility to proteolytic enzyme, leading to progressive destruction of the GBM with subsequent hematuria and proteinuria, glomerulosclerosis and ultimately end-stage renal disease. The current therapy is limited to dialysis and transplantation, with a higher risk of anti-GBM disease in the transplanted organs due to immune reaction against the type IV collagen chains.

Bone morphogenetic protein–7 (BMP-7) is a promising candidate to treat Alport syndrome. BMP-7 belongs to the TGF-β superfamily (10), and the kidney is the major site of BMP-7 expression during both embryogenesis and postnatal development (11). Pharmacological doses of BMP-7 can repair damaged renal tubules and preserve renal function in several models of renal diseases, including the Col4A3 knockout model of Alport syndrome (12–20). However, the exact role of endogenous BMP-7 and its mechanism of action remain unclear. In addition, the administration of recombinant BMP-7, whose target cells are widely expressed throughout the body, might also produce some undesired extrarenal effect.

The local activity of endogenous BMPs is controlled by certain classes of binding molecules that act as positive or negative regulators of BMP signaling activity (10, 21–24). BMP antagonists function through direct association with BMP, thus inhibiting the binding of BMP to its receptors and defining the boundaries of BMP activity.

The product of uterine sensitization–associated gene-1 (USAG-1) acts as a kidney-specific BMP antagonist, and USAG-1 binds to and inhibits the biological activity of BMP-7 (22, 25). USAG-1 is

Conflict of interest: The authors have declared that no conflict of interest exists.
Citation for this article: *J Clin Invest.* 2010;120(3):768–777. doi:10.1172/JCI39569.

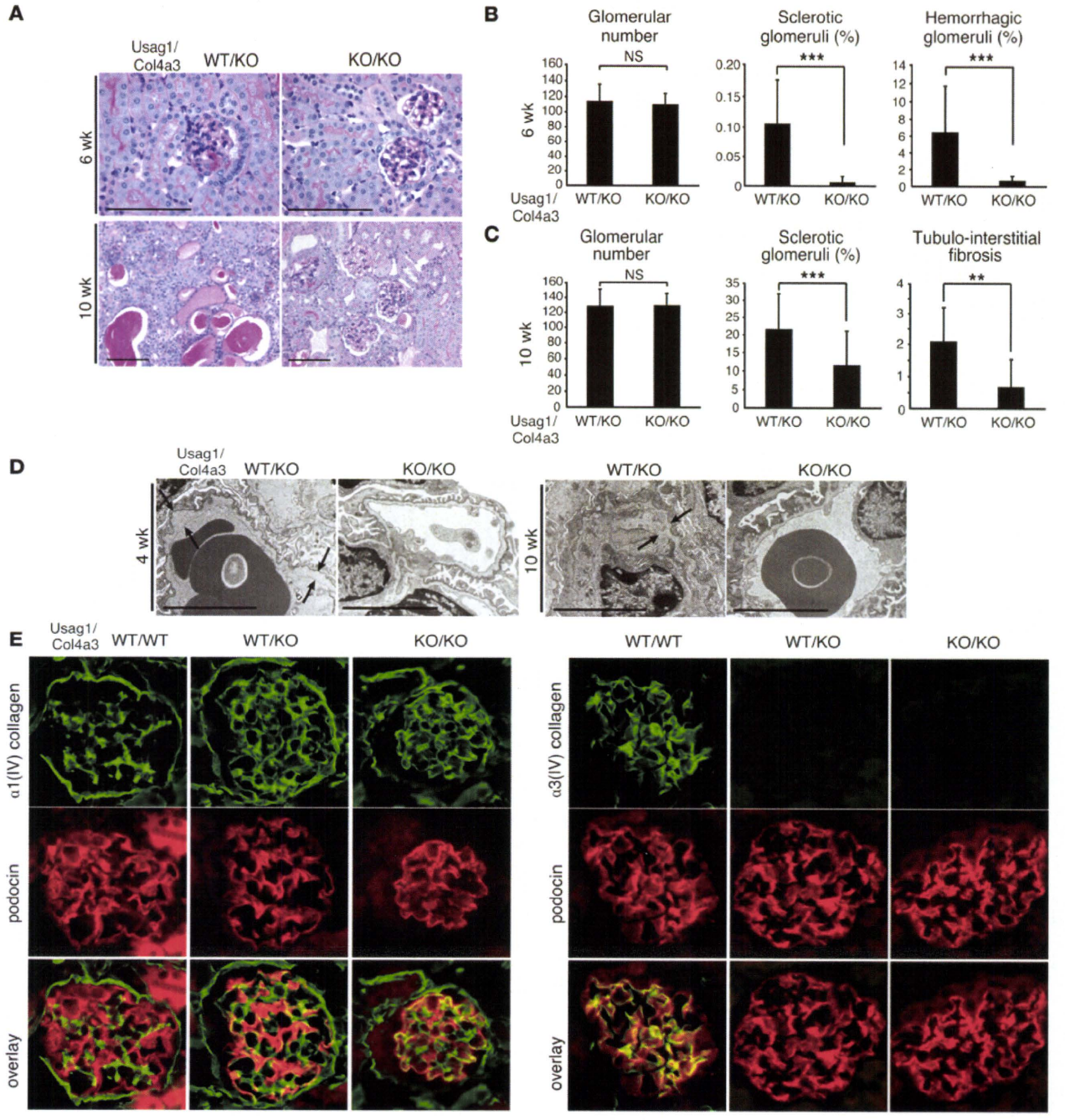

Figure 1

Usag1$^{-/-}$*Col4a3*$^{-/-}$ mice showed less glomerular and tubular injury. (**A**) Representative histological findings in *Usag1*$^{+/+}$*Col4a3*$^{-/-}$ mice (WT/KO) and *Usag1*$^{-/-}$*Col4a3*$^{-/-}$ mice (KO/KO) at 6 weeks and 10 weeks of age. Scale bars: 100 μm. (**B** and **C**) Quantitative assessment of the number of glomeruli, percentages of sclerotic and hemorrhagic glomeruli, and tubulointerstitial fibrosis score in *Usag1*$^{+/+}$*Col4a3*$^{-/-}$ mice (WT/KO) and *Usag1*$^{-/-}$*Col4a3*$^{-/-}$ mice (KO/KO) at 6 weeks (**B**, $n = 5$) and 10 weeks of age (**C**, $n = 10$). Bars indicate the mean ± SD. $^{**}P < 0.01$; $^{***}P < 0.05$. (**D**) Electron microphotographs in *Usag1*$^{+/+}$*Col4a3*$^{-/-}$ mice (WT/KO) and *Usag1*$^{-/-}$*Col4a3*$^{-/-}$ mice (KO/KO) at 4 weeks and 10 weeks of age. Arrows indicate the splitting of GBM. Scale bars: 5 μm. (**E**) Immunostaining for α1(IV) and α3(IV) collagen in the glomeruli of WT littermates (WT/WT), *Usag1*$^{+/+}$*Col4a3*$^{-/-}$ mice (WT/KO), and *Usag1*$^{-/-}$*Col4a3*$^{-/-}$ mice (KO/KO) at 6 weeks of age. Podocin was used as a podocyte marker. Note the positive staining for α1(IV) collagen along with the GBM of *Usag1*$^{+/+}$*Col4a3*$^{-/-}$ mice (WT/KO) and *Usag1*$^{-/-}$*Col4a3*$^{-/-}$ mice (KO/KO), while the staining is restricted to mesangial areas in the glomeruli of WT littermates.

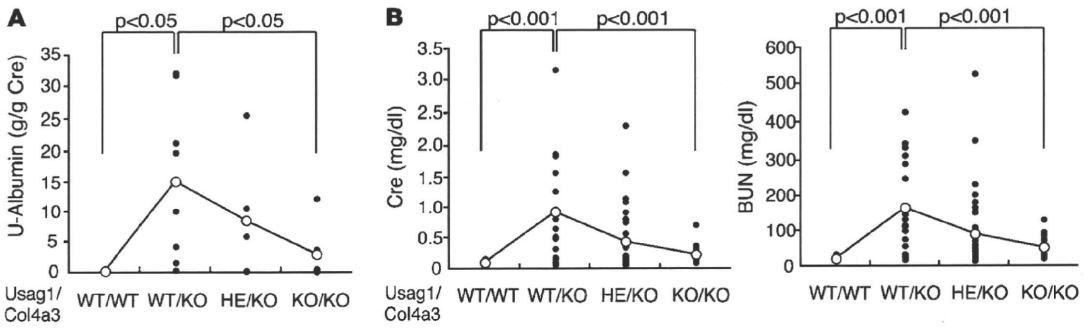

Figure 2

Usag1$^{-/-}$*Col4a3*$^{-/-}$ mice showed less albuminuria and preserved renal function. (**A**) Urinary albumin excretion normalized by urinary creatinine in WT littermates (WT/WT, $n = 4$), *Usag1*$^{+/+}$*Col4a3*$^{-/-}$ mice (WT/KO, $n = 8$), *Usag1*$^{+/-}$*Col4a3*$^{-/-}$ mice (HE/KO, $n = 5$), and *Usag1*$^{-/-}$*Col4a3*$^{-/-}$ mice (KO/KO, $n = 7$) at 6 weeks of age. Open circles represent mean value of each column, while closed circles represent individual mice. (**B**) Plasma creatinine and blood urea nitrogen (BUN) levels in WT littermates (WT/WT, $n = 20$), *Usag1*$^{+/+}$*Col4a3*$^{-/-}$ mice (WT/KO, $n = 18$), *Usag1*$^{+/-}$*Col4a3*$^{-/-}$ mice (HE/KO, $n = 34$), and *Usag1*$^{-/-}$*Col4a3*$^{-/-}$ mice (KO/KO, $n = 17$) at 10 weeks of age. Bars indicate mean ± SD. Open circles represent mean value of each column, while closed circles represent individual mice.

expressed in distal tubules and colocalizes with BMP-7 in distal convoluted tubules and connecting tubules (26). Furthermore, *Usag1*$^{-/-}$ mice are resistant to tubular injury such as acute renal failure and interstitial fibrosis, and USAG-1 is the central negative regulator of BMP function in the adult kidney (27). Because in adults the expression of USAG-1 is confined to the kidneys, targeting the activity of this protein might yield safer and more kidney-specific therapies than the administration of BMP-7 (23). For this, it will be important to first elucidate the role of USAG-1 in the pathology of progressive glomerular injury.

Here we show that genetic ablation of USAG-1 significantly attenuated the disease progression and preserved renal function in *Col4a3*$^{-/-}$ mice, a model for human Alport syndrome. The observations in this study suggest that USAG-1 might contribute to the pathogenesis of renal deterioration by a mechanism we believe to be novel that involves crosstalk between the macula densa of the distal tubules and the mesangium of the belonging glomerulus. In addition, we demonstrate that in the kidney of *Col4a3*$^{-/-}$ mice, TGF-β signaling includes phosphorylation of Smad1/5/8, transcription factors classically considered to be the downstream effectors of BMP signaling.

Results

Loss of USAG-1 slows progression of glomerular injury in Alport mice. *Col4a3*$^{-/-}$ mice, a mouse model of human Alport syndrome, develop progressive glomerulonephritis associated with tubulointerstitial fibrosis leading to renal failure. Kidneys from *Col4a3*$^{-/-}$ mice showed irregular thickening and splitting of the GBM at 4 weeks of age by electron microscopy. At 5 weeks of age, proteinuria is initiated, and at 6 weeks of age, minor glomerular lesion is occasionally observed by light microscopy. At 10 weeks of age, severe glomerular lesions associated with tubulointerstitial fibrosis are observed, and renal function deteriorates.

To test the role of USAG-1 in the progression of end-stage renal disease originating from glomerular injury, mice deficient in both *Col4a3* gene and *Usag1* gene were generated (*Usag1*$^{-/-}$*Col4a3*$^{-/-}$ mice). A histological examination of the kidneys from *Usag1*$^{+/+}$*Col4a3*$^{-/-}$ mice revealed segmental sclerosis and intraglomerular hemorrhage at 6 weeks of age, while these changes were almost completely absent in *Usag1*$^{-/-}$*Col4a3*$^{-/-}$ mice (Figure 1, A and B). At 10 weeks of age, *Usag1*$^{+/+}$*Col4a3*$^{-/-}$ mice demonstrated glomerulosclerosis associated with inflammatory cell infiltration, interstitial fibrosis, tubular atrophy, and cast formation, while these changes significantly decreased in *Usag1*$^{-/-}$*Col4a3*$^{-/-}$ mice (Figure 1, A and C).

An ultrastructural analysis of GBM using transmission electron microscopy at 4 weeks of age showed that *Usag1*$^{+/+}$*Col4a3*$^{-/-}$ mice had extensive splitting of the GBM, while *Usag1*$^{-/-}$*Col4a3*$^{-/-}$ mice showed almost normal GBM structure (Figure 1D). *Usag1*$^{-/-}$*Col4a3*$^{-/-}$ mice at 10 weeks of age also exhibited a significant preservation of GBM structure in comparison with age-matched *Usag1*$^{+/+}$*Col4a3*$^{-/-}$ mice (Figure 1D).

The immunostaining of α1(IV) or α3(IV) collagen was performed to compare the glomerular localization of α(IV) collagen in both genotypes (Figure 1E). The expression of α1(IV) collagen was detected in the GBM of both *Usag1*$^{+/+}$*Col4a3*$^{-/-}$ and *Usag1*$^{-/-}$*Col4a3*$^{-/-}$ mice, while the expression was confined to mesangial area in the WT mice. The expression of α3(IV) collagen was absent in the GBM of both *Usag1*$^{+/+}$*Col4a3*$^{-/-}$ and *Usag1*$^{-/-}$*Col4a3*$^{-/-}$ mice, while the expression was detected along the GBM in the WT mice. Therefore, regardless of the presence or absence of USAG-1, no alteration was observed in the glomerular localization of α(IV) collagen.

Usag1$^{-/-}$*Col4a3*$^{-/-}$ *mice showed less albuminuria, preserved renal function, and longer life span.* An analysis of urinary albumin excretion at 6 weeks of age is shown in Figure 2A, demonstrating significantly less albuminuria in *Usag1*$^{-/-}$*Col4a3*$^{-/-}$ mice than in *Usag1*$^{+/+}$*Col4a3*$^{-/-}$ mice. The systolic blood pressure of *Usag1*$^{-/-}$*Col4a3*$^{-/-}$ mice at 5 weeks of age was slightly lower than that of *Usag1*$^{+/+}$*Col4a3*$^{-/-}$ mice (Supplemental Figure 2; supplemental material available online with this article; doi:10.1172/JCI39569DS1). Renal function of *Usag1*$^{-/-}$*Col4a3*$^{-/-}$ mice at 10 weeks of age, as assessed by serum creatinine and blood urea nitrogen, was also significantly preserved in comparison with that of *Usag1*$^{+/+}$*Col4a3*$^{-/-}$ mice (Figure 2B), consistent with the results of renal histology and urinary albumin excretion. Furthermore, upon aging beyond 13 weeks, *Usag1*$^{-/-}$*Col4a3*$^{-/-}$ mice showed less mortality than *Usag1*$^{+/+}$*Col4a3*$^{-/-}$ mice (Supplemental Figure 1).

Inflammatory cytokine expression was significantly reduced in Usag1$^{-/-}$*Col4a3*$^{-/-}$ *mice.* As previously reported, the mRNA of inflammatory cytokines such as TNF-α, IL-1β, monocyte chemoattractant protein-1 (MCP-1), and TGF-β was upregulated in the kidneys of *Usag1*$^{+/+}$*Col4a3*$^{-/-}$ mice at 10 weeks of age (28, 29). In *Usag1*$^{-/-}$*Col4a3*$^{-/-}$ mice, however, increases in inflammatory cytokines were signifi-

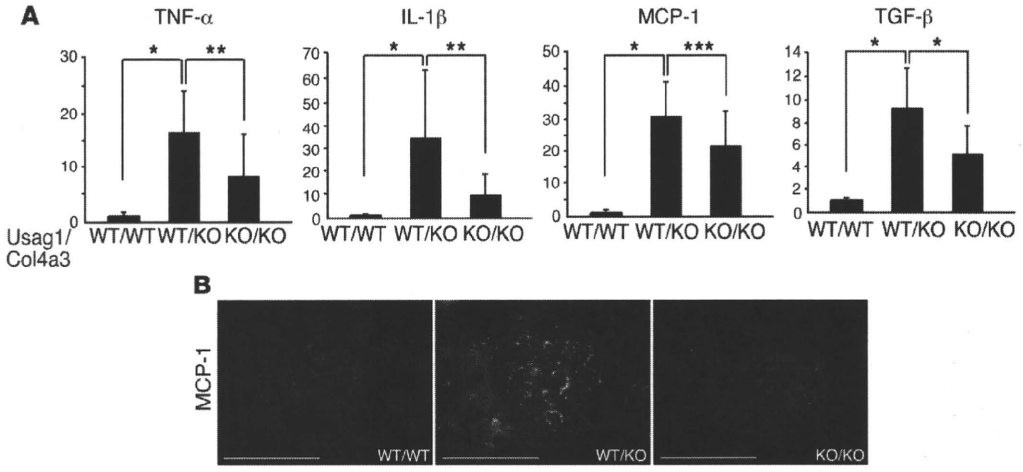

Figure 3

The expression of inflammatory cytokines significantly decreased in the kidneys of *Usag1*$^{-/-}$*Col4a3*$^{-/-}$ mice. (**A**) Real-time RT-PCR analysis of inflammatory cytokine mRNA in the kidneys of WT littermates (WT/WT), *Usag1*$^{+/+}$*Col4a3*$^{-/-}$ mice (WT/KO), and *Usag1*$^{-/-}$*Col4a3*$^{-/-}$ mice (KO/KO) at 10 weeks of age. The expression levels were normalized to those of GAPDH and expressed relative to those of WT littermates ($n = 10$). Bars indicate the mean ± SD. *$P < 0.001$; **$P < 0.01$; ***$P < 0.05$. (**B**) Representative immunostaining for MCP-1 in the kidneys of WT littermates (WT/WT), *Usag1*$^{+/+}$*Col4a3*$^{-/-}$ mice (WT/KO), and *Usag1*$^{-/-}$*Col4a3*$^{-/-}$ mice (KO/KO) at 10 weeks of age. Scale bars: 100 μm.

cantly attenuated (Figure 3A). Immunostaining for MCP-1 revealed faint expression of MCP-1 in the glomeruli of *Usag1*$^{-/-}$*Col4a3*$^{-/-}$ mice in comparison with *Usag1*$^{+/+}$*Col4a3*$^{-/-}$ mice (Figure 3B).

Enhanced Smad1/5/8 phosphorylation in Usag1$^{+/+}$*Col4a3*$^{-/-}$ *mice, but not in Usag1*$^{-/-}$*Col4a3*$^{-/-}$ *mice, was possibly activated by TGF-β signaling.* Next, the activation of Smad signaling was examined. The traditional view of the TGF-β superfamily signaling pathways assumes 2 distinct branches: a TGF-β branch that signals through Smad2/3 and a BMP branch that signals through Smad1/5/8 (30).

We observed increased phosphorylation of Smad2, the TGF-β signal transducer, in the kidneys of *Usag1*$^{+/+}$*Col4a3*$^{-/-}$ mice as compared with WT mice as well as *Usag1*$^{-/-}$*Col4a3*$^{-/-}$ mice (Figure 4A), consistent with high expression of TGF-β in *Usag1*$^{+/+}$*Col4a3*$^{-/-}$ mice (Figure 3A). The phosphorylation of Smad1/5/8, the classical BMP signal transducer, was expected to be reduced in the kidneys of *Usag1*$^{+/+}$*Col4a3*$^{-/-}$ mice due to generally low expression of BMP-7 in kidney disease models (12, 17, 26, 31). However, the phosphorylation of Smad1/5/8 was unexpectedly increased in the kidneys of *Usag1*$^{+/+}$*Col4a3*$^{-/-}$ mice in comparison with WT mice as well as *Usag1*$^{-/-}$*Col4a3*$^{-/-}$ mice.

Recently, several groups demonstrated that TGF-β activates Smad1/5 in addition to Smad2/3 in endothelial cells through novel receptor complexes (32–34). Thus, we hypothesized that the increased phosphorylation of Smad1/5/8 in the kidneys of *Usag1*$^{+/+}$*Col4a3*$^{-/-}$ mice might also have resulted from high expression of TGF-β. To test this hypothesis, we administered TGF-β to various types of cells including MDCK cells, primary mesangial cells, NRK cells (rat tubule epithelial cells), NIH3T3 cells, and HeLa cells, and demonstrated that TGF-β can activate the phosphorylation of Smad1/5/8 in addition to Smad2 in all these cell types (Figure 4B). The phosphorylation of Smad1/5/8 was induced by TGF-β at concentrations as low as 1 ng/ml (Figure 4C). Furthermore, the phosphorylation of Smad1/5/8 in the kidneys of *Usag1*$^{+/+}$*Col4a3*$^{-/-}$ mice correlated well with renal TGF-β as well as with serum creatinine levels, but not with the expression of BMP-7 (Figure 4D). Taken together, these results indicate that enhanced phosphorylation of Smad1/5/8 in *Col4a3*$^{-/-}$ mice might be due to TGF-β signaling and attenuated phosphorylation of Smad1/5/8 in *Usag1*$^{-/-}$*Col4a3*$^{-/-}$ mice might reflect reduced expression of TGF-β and disease severity.

Usag1$^{-/-}$*Col4a3*$^{-/-}$ *mice showed less expression and activity of MMPs in the kidneys.* Previous reports have demonstrated the important roles of MMPs in increasing susceptibility of defective Alport GBM to proteolytic degradation (9). The expression of *MMP* mRNA reported to be involved in this model was analyzed in the kidneys of 10-week-old mice, and this demonstrated strong upregulation of MMP-2, MMP-3, MMP-7, MMP-9, and MMP-12 in the kidneys of *Usag1*$^{+/+}$*Col4a3*$^{-/-}$ mice, while the expression of these MMPs was significantly less increased in the kidneys of *Usag1*$^{-/-}$*Col4a3*$^{-/-}$ mice (Figure 5A). The proteolytic activity of these MMPs in the kidney extracts was also determined by casein and gelatin zymography. Casein zymography showed a significant reduction in MMP-7 and MMP-12 activities (Figure 5B), and gelatin zymography demonstrated significant reduction of MMP-2 activity in the kidneys of *Usag1*$^{-/-}$*Col4a3*$^{-/-}$ mice in comparison with *Usag1*$^{+/+}$*Col4a3*$^{-/-}$ mice (Figure 5C). Also, the bands seen at 57 and 45 kDa in gelatin zymography, possibly representing MMP-3 activity (35), were significantly less in the kidneys of *Usag1*$^{-/-}$*Col4a3*$^{-/-}$ mice. Recently, it was demonstrated that expression of MMP-12 was markedly upregulated in the glomeruli of *Usag1*$^{+/+}$*Col4a3*$^{-/-}$ mice, and inhibition of MMP-12 preserved the integrity of GBM (29). Immunostaining for MMP-12 demonstrated a significant upregulation in the glomeruli and interstitium of *Usag1*$^{+/+}$*Col4a3*$^{-/-}$ mice, while the induction was attenuated in *Usag1*$^{-/-}$*Col4a3*$^{-/-}$ mice (Figure 5D). While MMP-12 is expressed by macrophages as well as glomerular cells such as podocytes (29, 36, 37), immunostaining of CD11b, a marker of monocytes and tissue macrophages, failed to demonstrate any significant infiltration of macrophages or monocytes in the glomeruli of 10-week-old *Usag1*$^{+/+}$*Col4a3*$^{-/-}$ mice (data not shown), suggesting that the glomerular MMP-12 in Alport mice was not due to the macrophages that infiltrated the glomeruli.

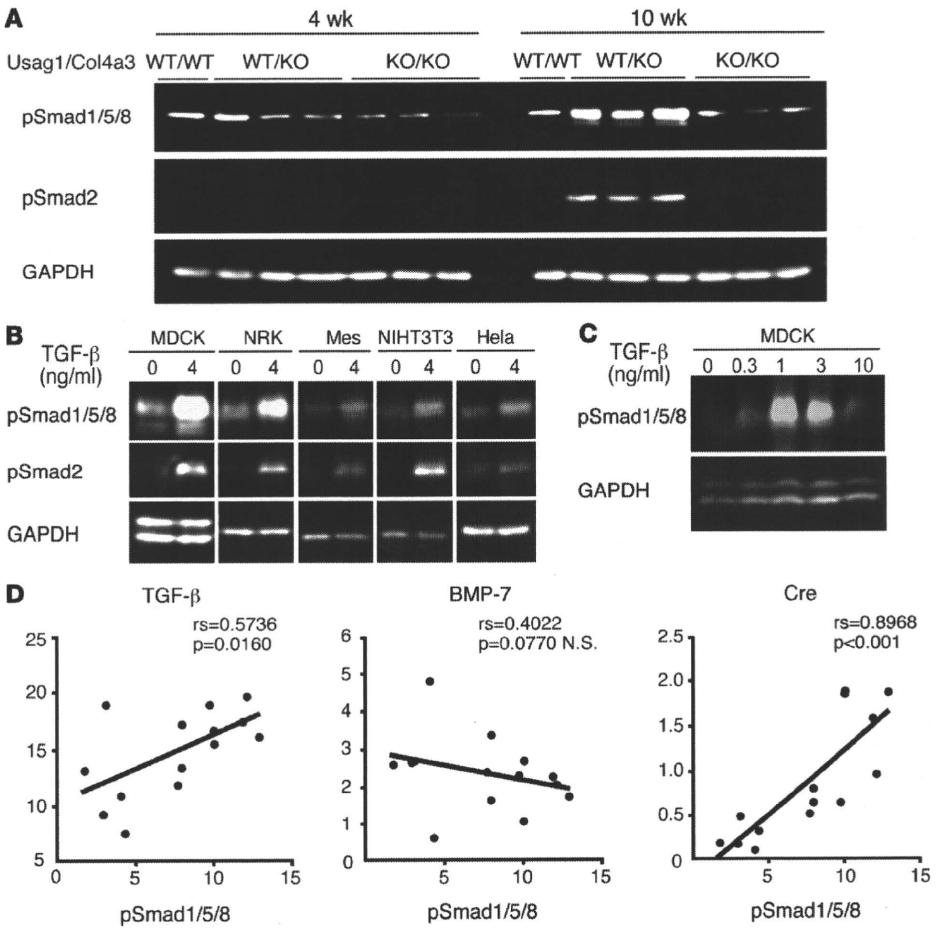

Figure 4
Smad1/5/8 phosphorylation was enhanced in *Usag1*$^{+/+}$*Col4a3*$^{-/-}$ mice, but not in *Usag1*$^{-/-}$*Col4a3*$^{-/-}$ mice. (**A**) Representative immunoblotting for Smad phosphorylation in the kidneys of WT littermates (WT/WT), *Usag1*$^{+/+}$ *Col4a3*$^{-/-}$ mice (WT/KO), and *Usag1*$^{-/-}$*Col4a3*$^{-/-}$ mice (KO/KO) at 4 and 10 weeks of ages. (**B**) A panel of cell lines were tested for the ability of TGF-β to induce phosphorylation of Smad1/5/8 in addition to Smad2. Cells were either left untreated or stimulated with 4 ng/ml of TGF-β for 1 hour. Whole-cell extracts were analyzed by immunoblotting using antibodies against phosphorylated Smad1/5/8 (pSmad1/5/8), pSmad2, and GAPDH as a loading control. (**C**) Representative immunoblotting showing the effect of various concentrations of TGF-β on the phosphorylation of Smad1/5/8 in MDCK cells. (**D**) Correlation between the phosphorylation levels of Smad1/5/8 in the kidneys of *Usag1*$^{+/+}$*Col4a3*$^{-/-}$ mice and mRNA expression of TGF-β and BMP-7 and serum creatinine (n = 14). The levels of phosphorylation of Smad1/5/8 were determined using the LAS image analysis system.

USAG-1 was not expressed in the Alport glomeruli. USAG-1 is expressed predominantly in the distal tubules, more specifically, in the thick ascending limb, distal convoluted tubules, and connecting tubules in adult kidneys, and not expressed in glomeruli (26). In situ hybridization was used to determine the expression of USAG-1 in *Usag1*$^{+/+}$*Col4a3*$^{-/-}$ mice and demonstrated that USAG-1 expression was not detectable in the glomeruli of *Usag1*$^{+/+}$*Col4a3*$^{-/-}$ mice either (Figure 6A) and was confined to tubules.

USAG-1 colocalizes with BMP-7 in the macula densa. Deficiency of USAG-1 significantly attenuated glomerular pathology in the *Col4a3*$^{-/-}$ mouse model of Alport syndrome in spite of the absence of USAG-1 expression in glomeruli. Further experiments focused on the part of the distal tubule that came in contact with its own glomerulus, the macula densa (Figure 6B). To determine whether USAG-1 is expressed in macula densa cells, we performed double staining of nNOS, a specific marker for macula densa, and β-gal using *Usag1*$^{+/LacZ}$ mice. As shown in Figure 6C, β-gal staining as well as immunostaining with anti-LacZ antibody colocalized with nNOS staining, indicating that USAG-1 was expressed in macula densa. BMP-7 is expressed in distal convoluted tubules, connecting tubules, collecting ducts, and podocytes (26). β-gal staining as well as immunostaining with anti-LacZ antibody also colocalized with nNOS in the kidneys of *Bmp7*$^{+/LacZ}$ mice, indicating the expression of BMP-7 in the macula densa (Figure 6C). Therefore, USAG-1 colocalizes with BMP-7 in the macula densa cells.

BMP-7 suppressed TGF-β–induced MMP-12 upregulation in mesangial cells, and USAG-1 antagonized the action of BMP-7. The macula densa, in which both USAG-1 and BMP-7 are expressed, is adjacent to mesangial cells in its own glomerulus (Figure 6B). To investigate potential mechanisms that are responsible for the beneficial effect of USAG-1 deficiency in Alport syndrome, the effect of BMP-7 and USAG-1 in cultured mesangial cells was examined. The expression of MMP-12 in cultured mesangial cells was upregulated by the administration of IL-1β and TGF-β, but not by the administration of MCP-1 (Figure 6D), in spite of the fact that MCP-1 is reported to stimulate MMP-12 expression in podocytes (29). The administration of BMP-7 suppressed TGF-β–induced MMP-12 upregulation in mesangial cells, and simultaneous administration of USAG-1 antagonized the suppressive effect of BMP-7 (Figure 6E). These results indicate that USAG-1 might enhance MMP-12 expression in the glomeruli by suppressing the inhibitory effect of BMP-7 and exacerbate glomerular disease progression in Alport syndrome.

Discussion

This study demonstrates that USAG-1 accelerates glomerular pathogenesis in a mouse model of human Alport syndrome, possibly through the crosstalk between the kidney tubules and its own glomerulus. *Usag1*$^{-/-}$*Col4a3*$^{-/-}$ mice demonstrated attenuated glomerular disease progression and preserved renal function in comparison with *Usag1*$^{+/+}$*Col4a3*$^{-/-}$ mice and significantly decreased

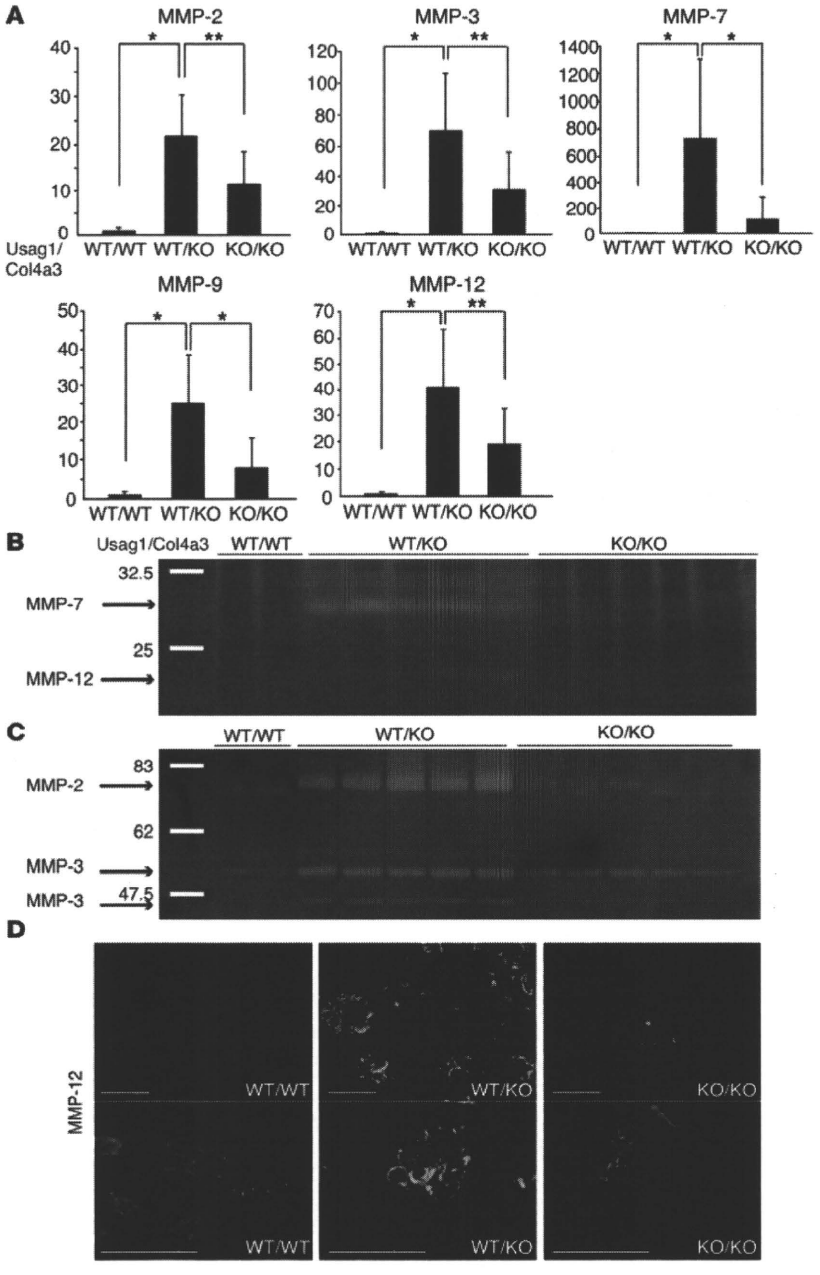

Figure 5

Usag1$^{-/-}$*Col4a3*$^{-/-}$ mice showed less expression and activity of MMPs in the kidneys. (**A**) Real-time RT-PCR analysis of MMP mRNA in the kidneys of WT littermates (WT/WT), *Usag1*$^{+/+}$*Col4a3*$^{-/-}$ mice, (WT/KO) and *Usag1*$^{-/-}$ *Col4a3*$^{-/-}$ mice (KO/KO) at 10 weeks of age. The expression levels were normalized to that of GAPDH and expressed relative to that in WT littermates ($n = 10$). Bars indicate the mean ± SD. $^{*}P < 0.001$; $^{**}P < 0.01$. (**B**) Casein zymography analyzing the kidneys of WT littermates (WT/WT), *Usag1*$^{+/+}$*Col4a3*$^{-/-}$ mice (WT/KO), and *Usag1*$^{-/-}$ *Col4a3*$^{-/-}$ mice (KO/KO) at 10 weeks of age. (**C**) Gelatin zymography analyzing the kidneys of WT littermates (WT/WT), *Usag1*$^{+/+}$*Col4a3*$^{-/-}$ mice (WT/KO), and *Usag1*$^{-/-}$*Col4a3*$^{-/-}$ mice (KO/KO) at 10 weeks of age. (**D**) Representative immunostaining for MMP-12 in the kidneys of WT littermates (WT/WT), *Usag1*$^{+/+}$*Col4a3*$^{-/-}$ mice (WT/KO), and *Usag1*$^{-/-}$*Col4a3*$^{-/-}$ mice (KO/KO) at 10 weeks of age. Scale bars: 100 μm.

expression and activity of MMPs, which play key roles in disease progression of Alport syndrome. Furthermore, USAG-1 and BMP-7 colocalized in the macula densa, a part of the distal tubules in contact with its own glomerulus, and BMP-7 reduced MMP-12 expression in mesangial cells, which was antagonized by USAG-1.

USAG-1 exacerbates glomerular injuries as well as tubular interstitial fibrosis. Tubular damage and interstitial fibrosis are the final common pathways leading to end-stage renal disease (ESRD) (38, 39) irrespective of the nature of the initial renal injury, and the degree of tubular damage parallels the impairment of renal function (39). Severe tubulointerstitial fibrosis is observed following glomerular injury in *Col4a3*$^{-/-}$ mice, and this exacerbates renal function. Because *Usag1*$^{-/-}$ mice were resistant to tubulointerstitial fibrosis (27), this resistance might contribute at least in part to the preservation of renal function in *Usag1*$^{-/-}$*Col4a3*$^{-/-}$ mice. In addition, *Usag1*$^{-/-}$ *Col4a3*$^{-/-}$ mice showed preserved GBM with less albuminuria in the early stage when tubular injury has yet to appear. Therefore, *Usag1*$^{-/-}$*Col4a3*$^{-/-}$ mice were resistant to both glomerular and tubular injuries.

USAG-1 increases the expression of MMP in Col4a3$^{-/-}$ *mice.* The molecular mechanisms by which the altered GBM composition in Alport syndrome causes renal pathogenesis remain unclear. It is proposed that abnormal persistence of α1/α1/α2(IV) collagen network in the adult GBM is associated with increased susceptibility to proteolysis by proteases in Alport syndrome (3, 9) and pharmacological ablation of MMP activities, especially MMP-12, leads to a significant attenuation in Alport disease progression (29, 40). The expression and activities of MMPs were significantly upregulated in the kidneys of *Usag1*$^{+/+}$*Col4a3*$^{-/-}$ mice, which is consistent with previous reports, and they were suppressed in the kidneys of *Usag1*$^{-/-}$*Col4a3*$^{-/-}$ mice. The suppression of MMP activities probably contributed, at least in part, to slow glomerular pathogenesis in *Usag1*$^{-/-}$*Col4a3*$^{-/-}$ mice. In addition, the administration of BMP-7 decreased the expression of MMP-12 in cultured mesangial cells, and USAG-1 antagonized the action of BMP-7. Therefore, USAG-1 might increase the expression of MMP in glomeruli and accelerate GBM destruction in *Col4a3*$^{-/-}$ mice.

Other possible roles of USAG-1 and BMP-7 in glomerular pathogenesis in Col4a3$^{-/-}$ *mice.* In addition to the inhibitory effect on MMP expression, BMP-7 possibly inhibits the progression of glomerular pathogenesis in *Col4a3*$^{-/-}$ mice at multiple steps. BMP-7 reduces the damage in podocytes (20, 41, 42) and mesangial cells (43–45) and attenuates the expression of inflammatory cytokines (46) and

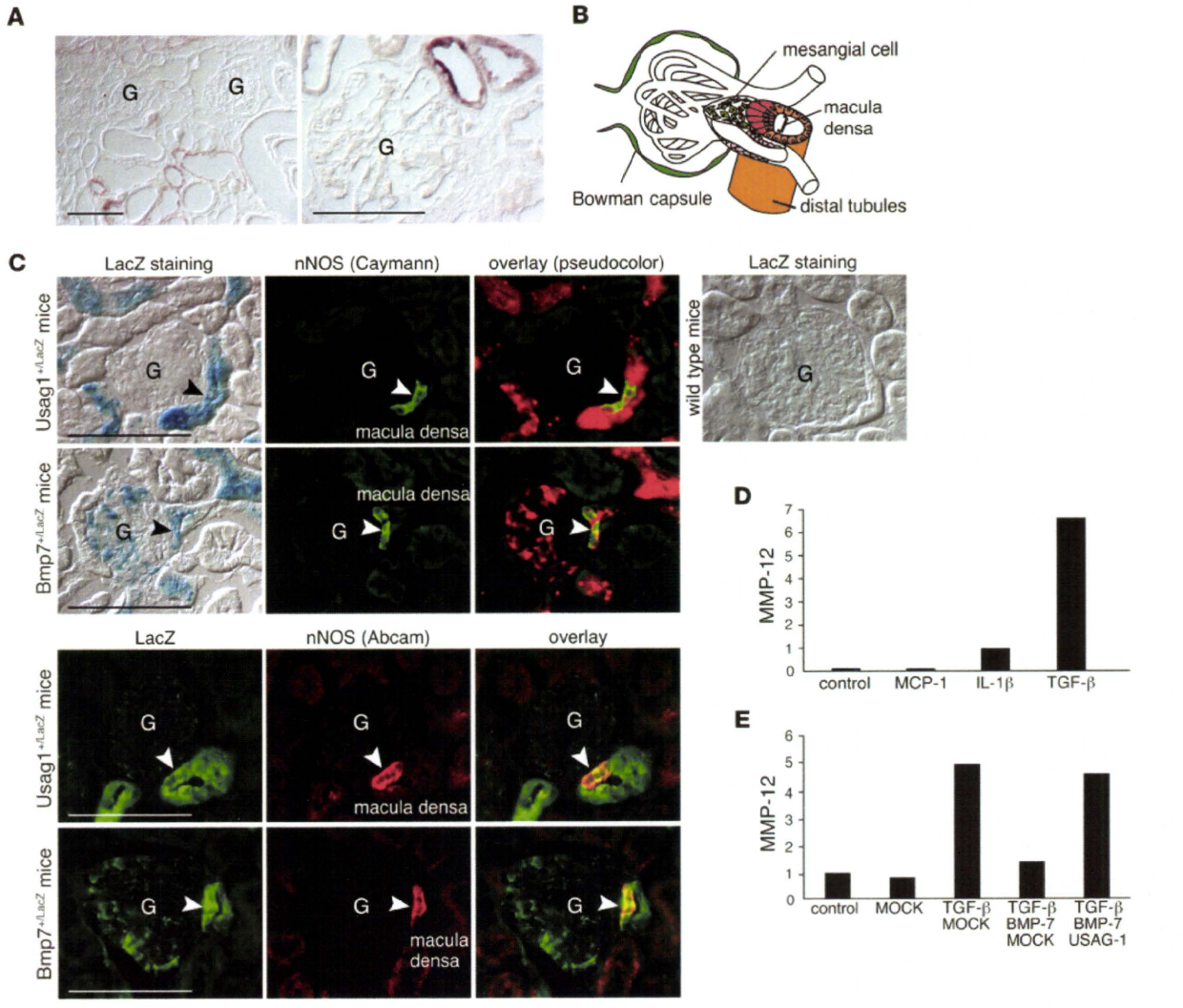

Figure 6

USAG-1 colocalizes with BMP-7 in the macula densa and inhibits the action of BMP-7 in mesangial cells. (**A**) In situ hybridization for USAG-1 mRNA in the kidneys of 10-week-old *Col4a3*$^{-/-}$ mice. Scale bars: 100 μm. G, glomerulus. (**B**) A schematic illustration of the juxtaglomerular apparatus. The macula densa is a part of distal tubules contacting with its glomerulus of origin and adjacent to mesangial cells. (**C**) β-Gal staining as well as immunostaining with anti-LacZ antibody colocalized with immunostaining with anti-nNOS (a marker for macula densa) antibody in the kidneys of *Usag1*$^{+/LacZ}$ mice and *Bmp7*$^{+/LacZ}$ mice. Kidney section from WT mice was also treated in the same way with the sections from *Usag1*$^{+/LacZ}$ mice and *Bmp7*$^{+/LacZ}$ mice and demonstrated no β-gal staining. Scale bars: 100 μm. (**D**) Real-time RT-PCR analysis of MMP-12 mRNA in cultured mesangial cells treated with inflammatory cytokines. The expression levels were normalized to those of GAPDH and expressed relative to those in controls. TGF-β markedly increased MMP-12 mRNA expression in mesangial cells. The graph reflects data that are representative for results of 4 independent experiments. (**E**) Real-time RT-PCR analysis of MMP-12 mRNA in cultured mesangial cells that were incubated with TGF-β, BMP-7, and USAG-1. BMP-7 suppressed TGF-β–induced MMP-12 upregulation in mesangial cells, and USAG-1 reversed the action of BMP-7. The graph reflects data that are representative for results of 4 independent experiments.

apoptosis in several types of cells (12, 41). Antagonizing the beneficial effects of BMP-7 by USAG-1 might enhance these injuries and accelerate glomerular pathogenesis in Alport syndrome.

USAG-1 secreted from distal tubules reaches the glomerulus and accelerates glomerular injury. Although the mechanism by which USAG-1 secreted from distal tubules reaches the glomerulus and exacerbates glomerular pathogenesis is not entirely clear, a crosstalk may exist between the distal tubule and the glomerulus in the same nephron.

The distal tubule of a nephron makes contact with the vascular pole of its glomerulus from which the distal tubule originated. At this point, there is a plaque of very specialized and differentiated cells in the distal tubule known as the macula densa (Figure 6B). The macula densa detects changes in the distal tubular fluid composition and transmits signals to the adjacent extraglomerular mesangial cells and afferent arterioles (47–53). Extraglomerular mesangial cells are anatomically in continuity with the glomerular mesangial cells and transmit the signal from the macula densa to the glomeru-